North American hydroclimate during past warms states: A proxy network-model comparison for the Last Interglacial and the mid-Holocene

Cameron B. de Wet[1], Daniel Enrique Ibarra[2], Bryce K. Belanger[1], and Jessica Leigh Oster[1]

[1]Vanderbilt University
[2]Brown University

November 23, 2022

Abstract

During the mid-Holocene (MH: ~6,000 years BP) and Last Interglacial LIG (LIG: ~129,000-116,000 years BP) differences in the seasonal and latitudinal distribution of insolation drove northern hemisphere high-latitude warming comparable to that projected in end-21st century low emissions scenarios, making these intervals potential analogs for future climate change in North America. However, terrestrial precipitation during past warm intervals is not well understood and PMIP4 models produce variable regional moisture patterns in North America during both intervals. To investigate the extent to which the latest generation of models reproduces moisture patterns indicated by proxy records, we compare hydroclimate output from 17 PMIP4 models with networks of moisture-sensitive proxies compiled for North America during the LIG (39 sites) and MH (257 sites). Agreement is lower for the MH, with models producing wet anomalies across the western United States (US) where a high concentration of proxies indicate aridity. The models that agree most closely with the LIG proxies differ from the PMIP4 ensemble by showing relative wetness in the eastern US and dryness in the northwest and central US. An assessment of atmospheric dynamics using an ensemble subset of the three models with the highest agreement suggests that LIG precipitation patterns are driven by weaker winter North Pacific pressure gradients and steeper summer North Pacific and Atlantic gradients. Comparison of this LIG subset ensemble with simulations of future low emissions scenarios indicates that the LIG may not be a sufficient analog for projected, end-21st century hydroclimatic change in North America.

North American hydroclimate during past warms states: A proxy network-model comparison for the Last Interglacial and the mid-Holocene

C. B. de Wet[1], D. E. Ibarra[2], B. K. Belanger[1], and J. L. Oster[1]

[1]Department of Earth and Environmental Sciences, Vanderbilt University, Nashville, TN, USA.

[2]Earth, Environmental, and Planetary Sciences, Brown University, Providence, RI, USA.

Corresponding author: Cameron de Wet (Cameron.de.wet@vanderbilt.edu)

Key Points:

- PMIP4 models agree more closely with moisture-sensitive North American proxy networks during the Last Interglacial than the mid-Holocene.
- A subset ensemble of three models maximizes agreement and suggests SLP gradient differences drove Last Interglacial precipitation patterns.
- The Last Interglacial may not be a sufficient analog for projected, end-21st century hydroclimatic change in North America.

Abstract

During the mid-Holocene (MH: ~6,000 years BP) and Last Interglacial LIG (LIG: ~129,000–116,000 years BP) differences in the seasonal and latitudinal distribution of insolation drove northern hemisphere high-latitude warming comparable to that projected in end-21st century low emissions scenarios, making these intervals potential analogs for future climate change in North America. However, terrestrial precipitation during past warm intervals is not well understood and PMIP4 models produce variable regional moisture patterns in North America during both intervals.

To investigate the extent to which the latest generation of models reproduces moisture patterns indicated by proxy records, we compare hydroclimate output from 17 PMIP4 models with networks of moisture-sensitive proxies compiled for North America during the LIG (39 sites) and MH (257 sites). Agreement is lower for the MH, with models producing wet anomalies across the western United States (US) where a high concentration of proxies indicate aridity. The models that agree most closely with the LIG proxies differ from the PMIP4 ensemble by showing relative wetness in the eastern US and dryness in the northwest and central US. An assessment of atmospheric dynamics using an ensemble subset of the three models with the highest agreement suggests that LIG precipitation patterns are driven by weaker winter North Pacific pressure gradients and steeper summer North Pacific and Atlantic gradients. Comparison of this LIG subset ensemble with simulations of future low emissions scenarios indicates that the LIG may not be a sufficient analog for projected, end-21st century hydroclimatic change in North America.

Plain Language Summary

The mid-Holocene and the Last Interglacial are the two most recent intervals that were warmer than the preindustrial and so are potentially useful analogs for future emissions scenarios. We compare the newest generation of climate models with North American precipitation patterns indicated by proxy records during the MH and LIG. We find that agreement is lower for the MH, with models producing wet anomalies across the western United States (US) where most records indicate drier conditions. Most LIG simulations show wetter conditions than the preindustrial in Alaska, northern Canada, and the southwestern US, yet the models that agree most closely with the LIG proxies also show eastern US wetness and Pacific Northwest and central US aridity.

Using a subset of the three models that most closely agree with the LIG proxy records, we find that differences in LIG sea level pressure gradients in the North Pacific and North Atlantic Oceans drove shifts in the spatial and seasonal distribution of precipitation across North America. We observe regional disagreement in precipitation patterns between this LIG subset ensemble and simulations of future emissions scenarios, suggesting that the LIG may not be a sufficient analog for projected, end-21st century hydroclimate changes in North America.

1 Introduction

Paleoclimate proxy records aggregated for specific intervals in Earth's geologically recent past offer valuable insight into spatiotemporal patterns of hydroclimate change (PAGES Hydro2k Consortium, 2017; Tierney et al., 2020). Comparison of moisture-sensitive proxy networks with paleoclimate model simulations can elucidate the driving mechanisms of past changes in rainfall and effective moisture (e.g., Harrison et al., 2003; Oster et al., 2015; Hermann et al., 2018; Otto-Bliesner et al. 2021; Feng et al. 2022). These comparisons are critical for the assessment of how well the current generation of models reproduce regional hydroclimate patterns suggested by proxy records and can help inform which models may be the most useful for predictions of future moisture availability across hydrologically sensitive regions in a warmer climate state (Tierney et al., 2020). Likewise, comparison of proxy records with climate models can help to refine the interpretations and clarify the biases associated with different proxy types, such as the influence of seasonality or the degree to which different timescales may be resolvable for a reconstructed climate signal (PAGES Hydro2k Consortium 2017).

The mid-Holocene (MH) (~6,000 years BP) and the Last Interglacial (LIG) period (~129,000–116,000 years BP) are the two most recent intervals with northern hemisphere temperatures comparable to low emissions scenarios for the end of the 21st century (Burke et al., 2018) and may offer glimpses of future hydroclimate in regions like North America. Despite similar greenhouse gas concentrations as the pre-industrial (PI), the MH may have been up to 0.7°C warmer than the PI (Marcott et al., 2013). However, recent estimates using data assimilation techniques indicate that global temperatures during the MH may instead have been similar to the PI (Osman et al., 2021). Nonetheless, orbitally driven differences in the seasonal and latitudinal distribution of incoming solar radiation during the MH relative to the modern drove an enhanced seasonal temperature gradient in North America and likely led to strengthened northern hemisphere (NH) monsoons (Otto-Bliesner et al., 2017). Peak global mean LIG surface temperatures (127–125 ka) are estimated to have been ~0.5°C (± 0.3°C) warmer than those of the PI (Hoffman et al., 2017) with the greatest warming occurring in the mid- and high latitudes (Turney and Jones, 2010). Like the MH, the LIG had greenhouse gas concentrations roughly equivalent to the pre-industrial (Otto-Bliesner et al., 2017), but even larger seasonal differences in the distribution of insolation than those of the MH, which drove a warmer Arctic (Turney and Jones, 2010), smaller ice sheets, and sea level that was ~6–9 meters higher than present (Dutton et al., 2015).

With the inclusion of both MH and LIG simulations as Tier-1 experiments in the current CMIP6/PMIP4 modeling efforts (Otto-Bliesner et al., 2017), the organization of updated MH and LIG proxy networks for robust comparison with model output is of significant utility for the paleoclimate community, as well as for planners preparing for future warming (Tingstad et al., 2014; Woodhouse et al., 2016). Importantly, regional terrestrial rainfall and moisture balance dynamics during past warm intervals are even less well understood than temperature variations (Scussolini et al., 2019; Otto-Bliesner et al., 2021; Tierney et al. 2020), partially due to the heterogenous geographic response of the water cycle to past global climate forcing (e.g., Greve et al., 2014; Scheff 2018), including in the western United States (Ibarra et al., 2018). Here we present and discuss aggregated networks of hydroclimate-sensitive proxy records for North America (Figure 1), where PMIP4 models produce highly variable regional precipitation patterns during both the MH and LIG. We statistically compare our proxy networks with annual precipitation and runoff output from 17 individual models, as well as model ensembles, for both time slices to investigate the degree to which the latest generation of climate model simulations reproduces the moisture patterns indicated by the proxy record. We then use a subset ensemble of the three models that agree most closely with the LIG proxy record to investigate the role of atmospheric dynamics in driving rainfall patterns during the LIG and to assess the degree to which the LIG may provide a useful analog for North American hydroclimate in projected, end-21st century warming scenarios.

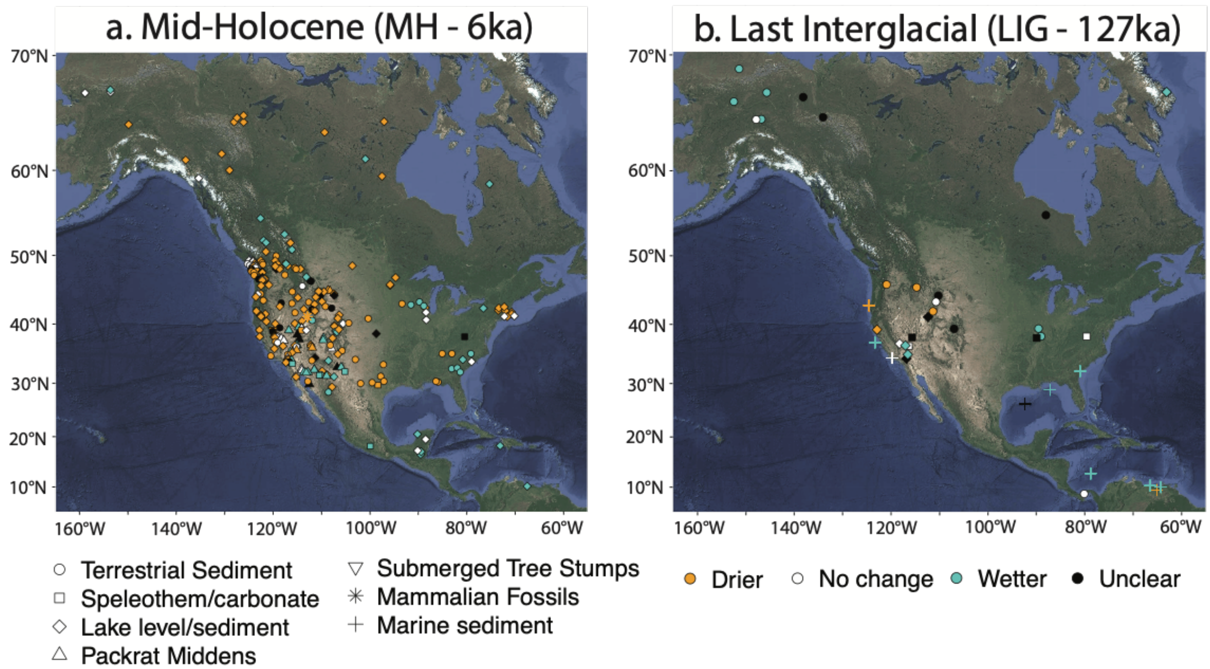

Figure 1. Mid-Holocene (a) and Last Interglacial (b) proxy networks for North America designated by the type of archive (symbol) and moisture designation relative to the pre-industrial for the Mid-Holocene and relative to the Holocene/modern for the Last Interglacial (color).

2 Methods

2.1 Proxy Networks

We compiled networks of moisture-sensitive proxy records for the MH (Figure 1a; Table S1) and LIG (Figure 1b; Table S2) respectively from the published literature for North and Central America (5° to 70°, 190° to 310°). Decades of research in the western US have resulted in dense proxy record coverage for this region during the MH, but the coverage is limited across much of Canada, the south-central US, and Central America (Thompson et al., 1993; Bartlein et al., 1998; Hermann et al., 2018). Our MH network includes 257 records, compiling and building on previously published regional networks including Thompson et al (1993) and Hermann et al. (2018) for western North America, Metcalfe et al. (2015) for the south-west US and Mexico, Gavin and Brubaker (2015) and Steinman et al. (2016) for the Pacific Northwest, and Sundqvist et al. (2014) for Canada and Alaska. The MH network includes proxies from lake sediments, packrat middens, speleothems, and pollen records, as well as one record from submerged tree stumps (Lindstrom, 1990) and one of mammal fossils (Grayson, 2000).

Proxy records for the LIG are sparse and unevenly distributed in North America, with the Western US and Alaska having the best spatial coverage (Scussolini et al., 2019; Otto-Bliesner et al., 2021). This is in large part because the LIG at 129,000 to 116,000 years BP is beyond the limit of radiocarbon dating (~50,000 years BP), complicating the development of well-constrained chronologies for paleoclimate archives. Our LIG network for North America includes 39 records, expanding the work of Scussolini et al. (2019), which included 19 records from North America. Our LIG network consists of lake sediments, marine sediments, speleothems, landscape features, and river-cut exposures. We include two marine sediment cores from the southern Caribbean Sea as they are interpreted as representing shifts in the mean ITCZ position. For the purposes of comparison, we consider the part of the record that the original authors identify as the warmest part of MIS5 or MIS5e specifically to represent the LIG.

For both time periods, we categorize proxy records as drier (D) or wetter (W) conditions or no change (N) in annual moisture based on the original author's interpretation of the moisture signal (Table S1, S2). For the MH, our moisture designations are evaluated for the period 6.0 +/- 1.0 ka relative to the pre-industrial. For the LIG, this moisture designation is made relative to the Holocene/modern record at a given site or within the record. For both intervals, we also include records for which no moisture signal can be interpreted due either to poorly resolved chronologies or an original interpretation of the moisture signal as representing non-local conditions, coding them as inconclusive (Figure 1). In our MH proxy network 53 sites are identified as wetter, 140 as drier, 38 exhibit no change, and 25 are considered inconclusive. In our LIG network 16 proxy sites are identified as wetter, 6 as drier, and 7 as no change in moisture signal, with 10 inconclusive. In sum, our LIG network contains 13 new records that were not included in the Scussolini et al. (2019) compilation and that are not designated as inconclusive, increasing the utility of the LIG proxy network for comparison with model output.

2.2 Model Output

We compare the MH and LIG proxy networks with output of monthly climatologies from 17 PMIP4 climate models of MH (6ka) and LIG (127ka) simulations accessed via the World Climate Research Programme (https://esgf-node.llnl.gov/search/cmip6/) (Table S3). Of the 17 models used, one (CNRM-CM6-1) provides monthly output for the LIG but not the MH and two (MPI-ESM1-2-LR, MRI-ESM2) provide monthly output for the MH but not the LIG. Simulation of terrestrial hydroclimate can differ between Earth system models due to differences in model resolution, land-surface models of water partitioning, albedo representations and energy budget schemes, as well as complexity in cloud microphysics controlling precipitation rates, large-scale circulation patterns and orographic precipitation (e.g., Delire et al., 2002; Dai, 2006; Trenberth, 2011; Dalmonech et al., 2015). We calculate annual precipitation percent anomaly by subtracting annually averaged monthly precipitation (*pr*) output for the pre-industrial (0ka) run from either the MH (6ka) run or the LIG (127ka) run and the *pr* output for the end of the 21st century (2071-2100) from two shared socioeconomic pathway (SSP) simulations (SSP2-4.5 and 5-8.5) from the historical (1850-1949) simulation in the native model resolution. We calculate annual percent runoff anomaly by subtracting annually averaged monthly evapotranspiration output (*evspsbl*) from the annually averaged monthly *pr* output for the LIG and MH relative to the pre-industrial (e.g., Oster et al., 2015; Hermann et al., 2018; Ibarra et al., 2018). In addition to comparisons between the proxy networks and annually averaged precipitation and runoff anomalies, we compare the proxy data with average precipitation and runoff percent anomalies for the winter half-year (NDJFMA) and summer half-year (MJJASO).

2.3 Agreement Coefficients

We compare hydroclimate changes simulated by each model at each proxy site with the change observed in the proxy networks by using the Gwet's AC2 statistic (Eq. 1) for categorical agreement between two raters (proxies and models) which classify items (sites) into categories (wetter, drier, no change) relative to the probability of random chance agreement (Gwet, 2008; Gwet, 2015; Conroy et al., 2019; Feng et al., 2022). The AC2 statistic is given by

(Eq. 1) AC2 = Pa - Pe1 - Pe

Where P_a is the percentage of agreement between the proxies and the model output and P_e is the expected percentage of agreement between the two due to chance alone. If models and proxy data are in complete agreement, then the AC2 agreement coefficient will be equal to 1. If there is no agreement between the two beyond what is expected by random chance, then the AC2 will be equal to 0. Opposite agreement between the models and proxy data (i.e., the model indicates wetter conditions at every site where the proxies suggest drier and vice versa) would be represented by an AC2 of -1. The Gwet's AC2 statistic weights observations based on the degree of model-proxy agreement by multiplying a matrix of the model-proxy observations by a weight matrix in which strong agreement (e.g., both the model and proxy indicate wetter conditions at a particular site) is given a weight of 1, strong disagreement (e.g., the model indicates drier conditions, the proxy indicates wetter) is given a weight of 0, and weak disagreement (e.g ., the model indicates drier, the proxy indicates no change) is given a weight of 0.5. To identify maximum possible agreement between each model and the proxy networks we vary the threshold value for a change in *pr* or runoff to be considered wetter or drier from 1 to 20% in 1% increments. For example, at a threshold of 10%, a model must simulate MH precipitation ≥ 110% of the PI for a site to be classified as wetter and ≤ 90% of the PI to be classified as drier. We chose a maximum rainfall threshold of 20% because this value encompasses the range of average relative standard deviations of simulated pre-industrial annual precipitation for North American grid cells from each model.

For comparison, we also present the Gwet's AC1 and the weighted Cohen's kappa (K_w) statistic, which has been used by similar proxy network-model comparison studies (e.g., DiNezio and Tierney, 2013; Oster et al., 2015; Oster and Ibarra, 2019), including for the MH (Hermann et al. 2018). K_w weights observations based on the degree of model-proxy disagreement, allowing for the presence of weak disagreement to positively influence the statistic in a similar fashion to Gwet's AC2. Gwet's AC1 is the first-order version of Gwet's AC2 and does not weight observations. That is, weak disagreement is considered mathematically identical to strong disagreement. Our calculated AC2 values tend to be higher than both K_w and AC1. We focus our discussion on our AC2 calculations because it takes weak disagreement into account, which AC1 does not. Additionally, AC2 is understood to be a more reliable metric than K_w for the degree of agreement between rates in the presence of high agreement and high prevalence of one category (e.g. Wongpakaran et al., 2013; Gwet, 2015).

3 Results

3.1 Mid-Holocene proxy network observations

The moisture patterns shown by our updated MH proxy network (n = 188 records in western North America) are largely consistent with observations from Hermann et al. (2018) (n = 170 records) and Thompson et al. (1993) (n = 99) for western North America. The western US, where moisture patterns are dominated by winter westerly storm-sourced rainfall, is characterized by increased aridity during the MH relative to the PI. As in Hermann at al. (2018), central and northern California, the Pacific Northwest, and the northern Rocky Mountain regions are consistently drier than the modern, while the Great Basin and southern Rockies exhibit both wet and dry sites and sites with no change (Figure 1a). Areas in the southwestern US and northern Mexico where the North American Monsoon contributes significantly to annual rainfall show a mixed response. Most sites along the US-Mexico border indicate increased MH wetness, whereas sites from northern New Mexico and northern Arizona suggest enhanced aridity.

We expand on the geographical range of the network from Hermann et al. (2018) (25°N to 55°N, 100°W to 130°W) by including proxy archives from across North America (5°N to 70°N, 190°W to 310°W), though the proxy coverage is more sparse outside of the western US due to taphonomy and preservation bias favoring arid regions versus wetter regions (Figure 1a). Modern precipitation patterns become less seasonal east of the Rocky Mountain and western Great Plains regions, with a roughly equal distribution of summer and winter moisture (Lora and Ibarra, 2019; Schneider et al., 2011; PRISM Climate Group, 2010). Archives from the Plains region in Texas and the Florida Panhandle demonstrate aridity ($n = 8$), as do several archives from southern New England ($n = 10$). Meanwhile, archives from the Carolinas and coastal Georgia indicate greater wetness during the MH ($n = 6$). A collection of sites in the upper Midwest shows a mixed response ($n = 9$). All the sites that we include from the Yucatan Peninsula, Central America, and the Caribbean region indicate wetter conditions or no change ($n = 9$). In Canada, southern British Columbia was drier along the border with the US ($n = 5$), with wetter conditions further north ($n = 5$). Drier conditions are observable in the Yukon and the Northwest Territories, and southern Nunavut ($n = 12$), aside from one wetter site in central Canada. Sites from Alaska display a mixed response with two showing no change, one wetter, and one drier ($n = 4$).

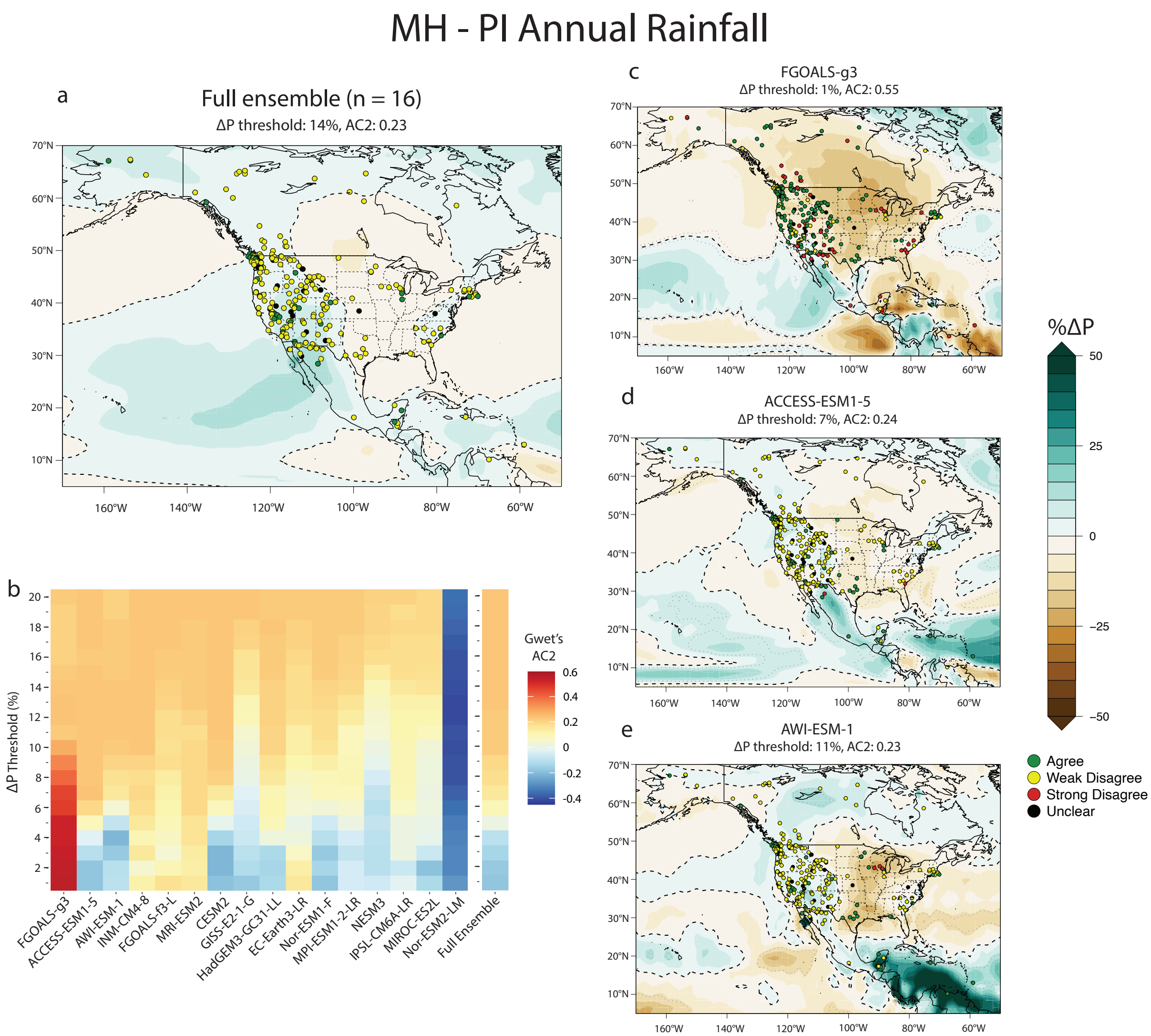

Figure 2. (a) Annual MH-PI precipitation anomaly (%ΔP) for the full PMIP4 ensemble (n=16) with MH proxy network plotted based on agreement with the ensemble climatology. (b) Heat map showing AC2 values at each threshold (1-20%) for the MH-PI annual precipitation anomaly to be considered wetter, drier, or unchanged. (c - d) Annual MH-PI precipitation anomaly (%ΔP) with MH proxy network plotted based on agreement with the underlying model climatology for three representative models (c: FGOALS-g3, d: ACCESS-ESM1-5, e: AWI-ESM-1). Dark gray dashed lines denote the boundary between positive and negative precipitation anomalies. Light gray dotted lines denote the threshold for the change in precipitation to be considered wetter, drier, or unchanged based on optimized agreement with the proxy network.

3.2 Mid-Holocene proxy network – model comparisons

Overall, agreement between the MH proxy network and model simulations is low for both annual precipitation (Figure 2b, Figure S1) and runoff (Figure S1). The full PMIP4 MH ensemble produces an AC2 value of 0.23 at a rainfall threshold of 13% (Figure 2a). Fourteen of the 16 models that provide MH output produce AC2 agreement coefficients between 0.19 and 0.24, with optimized rainfall thresholds that range from 7% to our maximum allowable value of 20%, and nine of the 16 models optimized at a threshold of 16% or higher (Figure 2b). These simulations show wetter MH conditions relative to the modern along the western US-Mexico border, where proxies also indicate enhanced wetness. However, most models also show some pattern of enhanced wetness over all or part of California, the Great Basin, the Pacific Northwest, and the Colorado Plateau, where a high concentration of archives generally indicate enhanced MH aridity. Since the wet anomaly in the simulations tends to be relatively modest (generally less than 20% wetter than the PI) our algorithm maximizes agreement by increasing the rainfall threshold such that most western US dry sites are categorized as weakly disagreeing with the lack of significant hydroclimate change in most of the simulations. Thus, the MH simulations for which agreement in the western US is optimized by increasing the precipitation threshold also tend to produce weak disagreement with wetter or drier archives across other regions in North America where modeled changes are small, such as the eastern US and Great Plains. ACCESS-ESM1-5 (Figure 2d) and AWI-ESM-1 (Figure 2e) are exceptions in that they produce the second and third highest AC2 and are optimized at relatively lower threshold values of 7% and 11% respectively. However, agreement for ACCESS-ESM1-5 and AWI-ESM-1 is only marginally higher than most of the other models for which all or most locations are characterized as 'no change'. One model, Nor-ESM2-LM, produces a large wet anomaly along the western coast of Canada that extends down into the western US, driving widespread disagreement with the proxy network and negative AC2 value that is not considered statistically significant ($p = 2$) (Figure S1).

FGOALS-g3 stands out in our MH comparisons with an AC2 value of 0.55 at a rainfall threshold of 1% and 0.52 or higher at a threshold of 5% or less (Figure 2c). This is driven by widespread aridity across most of the US and Canada and thus good agreement with the large concentration of "drier" proxy sites in the western US. Additionally, FGOALS-g3 produces wet anomalies in southern California and southwestern Arizona, driving good agreement with the wetter archives along the western portion of the US – Mexico border. However, this wet anomaly in the simulation does not extend east to the numerous wet sites in southeastern Arizona, northern Mexico, and southern New Mexico. Indeed, the rest of the US and most of Canada are characterized by aridity, driving agreement with concentrations of drier proxy sites in Texas, the northeast, and parts of the Midwest, as well as northwest Canada, but disagreement with the enhanced wetness of the Yucatán Peninsula, southeast US, and southern Wisconsin sites.

Kw values are lower than AC2 values for all models, ranging from 0.19 to -0.044, and are identified as not statistically significant for eight of the 16 models analyzed. AC1 values are also lower than AC2 values for all MH simulations, ranging from 0.51 to -0.09. Our calculated AC1 values for 11 of the 16 MH simulations are identified as not significant ($p > 0.05$) (Table S3). Thus, we focus on the MH AC2 values in our discussion.

3.3 Last Interglacial proxy network observations

LIG proxy records from the western US document drier conditions across the Pacific Northwest and northern Rockies and increased wetness in the southwest (Figure 1b; Table S2 and references therein). Marine sediment cores, the chronologies for which are tuned to SPECMAP (Pisias et al., 1984), indicate drier conditions along the Oregon coast and wetter conditions or conditions similar to today along the California coast (Pisias et al., 2001; Heusser et al., 2000; Lyle et al., 2010). The chronologies for the various western US lake records are also largely controlled by correlations to SPECMAP due to being well beyond the effective dating range for radiocarbon. These records track vegetation changes and shifts in lake water levels, with lakes from the northern US Rockies (Jiménez-Moreno et al., 2007), the Pacific Northwest (Whitlock and Bartlein, 1997), and northern California (Adam and West, 1983) indicating relative aridity during the LIG, while Great Basin lakes document wetter conditions or conditions similar to the present (Rehies et al., 2012; Forester et al., 2005; Woolfendon, 2003). Other lake records from the Yellowstone area (Baker, 1986), the Colorado Rockies (Anderson et al., 2014; Miller et al., 2014; Sharpe and Bright, 2014), northern Utah (Balch et al., 2005), and southern California (Glover et al., 2017) do not display clear signals of LIG hydroclimate.

Much of the existing literature for MIS5e climate conditions in Alaska focuses on temperature reconstructions as opposed to moisture conditions. However, it is hypothesized that warmer temperatures during the LIG drove wetter conditions across Alaska by increasing atmospheric water vapor content and accelerating the regional hydrologic cycle, as well as by decreasing the proportion of precipitation that fell as snowfall during shortened Arctic winters (CAPE Last Interglacial Project Members, 2006; Miller et al., 2010). We identify four Alaskan proxy sites across the central and northern portions of the state that indicate wetter LIG conditions based on pollen assemblages in lake cores (Muhs et al., 2001; CAPE Last Interglacial Project Members, 2006; Bigelow et al., 2014), river cut exposures (Bigelow et al., 2014), or paleosol data, as well as one soil record that indicates no change in moisture (Pewe et al., 1997). We also identify two sites, a record of soil formation (Tarnocai, 1990) and of pollen, plant fossils, and insect remains from a river bluff (Schweger and Matthews, 1991), that suggest warmer, but not necessarily wetter conditions in the Yukon region of western Canada. There are relatively few LIG records available for the rest of mainland Canada, likely due to the erosive nature of the Laurentide ice sheet during the last glaciation (LIGA Members, 1991). We identify one record of amino acids, pollen, and microfossils in buried organic sediments from the Hudson Bay lowlands that is suitable for inclusion in our network based on the continuous chronology, but which displays an uncertain climate signal at the LIG (Wyatt, 1990; LIGA Members, 1991).

Of the few LIG proxy records that exist from the eastern US, the majority indicate increased moisture. However, the poor proxy record coverage limits our ability to make broad-scale interpretations of hydroclimate changes for this region. Pollen records from two southern Illinoisan lakes document shifts to more temperate deciduous forests during the LIG and have been interpreted as indicative of wetter conditions relative to the present (Teed, 2000; Curry and Baker, 2000). Alkenes, $\delta^{13}C$, and $\delta^{18}O$ in plant leaf waxes in a northern Gulf of Mexico marine sediment core and terrestrial pollen fluctuations in a core off the coast of South Carolina and Georgia indicate that wetter than modern conditions persisted in the southeastern US during the LIG (Limoges et al., 2014; Suh et al., 2019). Changes in geochemistry and mineralogy in marine sediment core MD02-2549 from the north central Gulf of Mexico suggest changes in sediment provenance and relative contributions from different sub-basins, indicating a northeast migration of the main rainfall belt over the Mississippi River basin in response to greater boreal summer insolation of the LIG (Montero-Sessano et al. 2011). While this hypothesis is consistent with the increased wetness observable in Illinoisan lakes (Teed, 2000; Curry and Baker, 2000), we opt to code this core site as unclear in our proxy network because the signal interpreted by Montero-Serrano et al. (2011) is highly non-local. Additionally, two LIG speleothem records show no change in moisture conditions in western Virginia (Springer et al., 2014) and an inconclusive moisture signal in southeastern Missouri (Knight et al. 2006).

We identify one Central American soil record and two Caribbean Sea marine sediment cores that meet our criteria for inclusion in the LIG network. Pollen data from the U/Th-dated soil record of El Valle, Panama is indicative of hydroclimate conditions similar to that of today (Cárdenes-Sandí et al., 2019), while Mg/Ca and $\delta^{18}O$ data from the proximal SPECMAP-tuned ODP Core 999A have been interpreted as indicating lower sea surface salinity than the present and wetter conditions at the LIG (Schmidt and Spero, 2011), though Scussolini et al. (2019) note that the signal is weak and uncertainty is large in the record. Ribolleau et al. (2014) interpret sedimentological variations in a Cariaco Basin core to indicate less rainfall over the Unare river basin and more rainfall over the Tuy and Neveri river basins during the LIG. The authors argue the LIG preference for enhanced rainfall over the more northern Tuy and Neveri Basins indicates a northern shift of the ITCZ and rain belts compared to the Holocene (Ribolleau et al. 2014). Here we adopt the approximate locations of the river basins from Scussolini et al. (2019) for the purpose of plotting the sign of change at the sites.

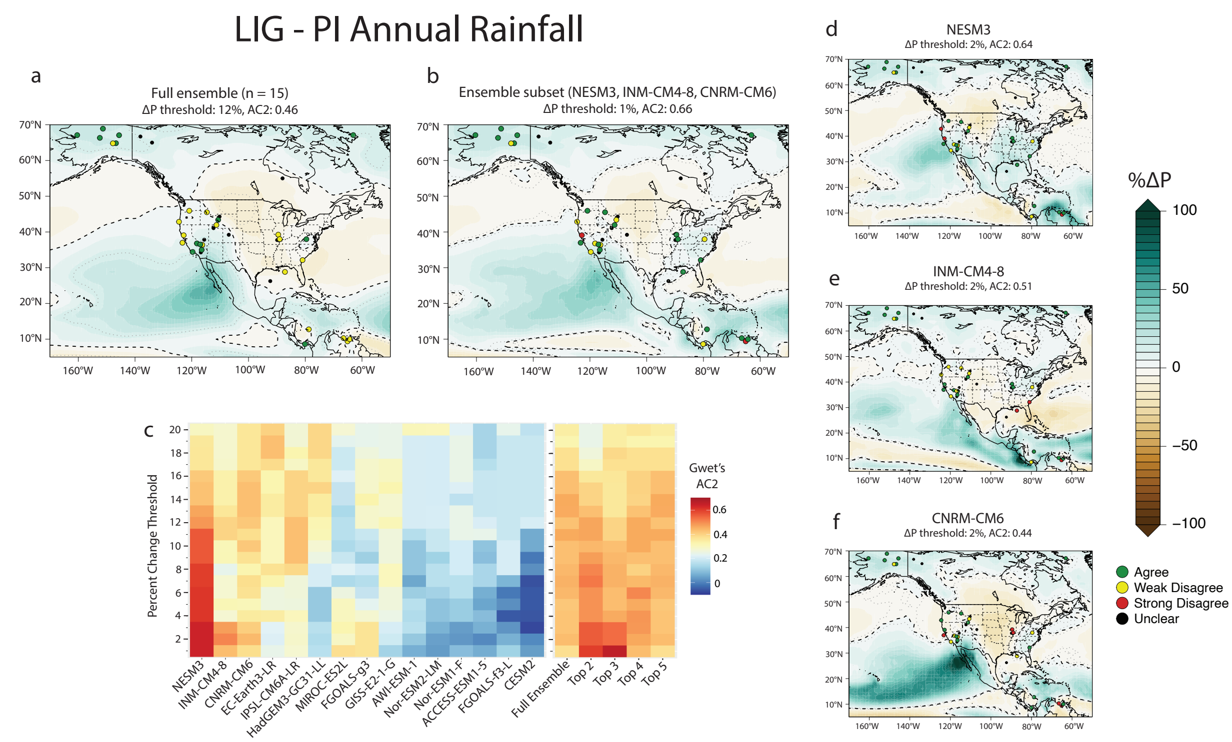

Figure 3. (a) Annual LIG-PI precipitation anomaly (%ΔP) for the full PMIP4 ensemble (n=15) with LIG proxy network plotted based on agreement with the ensemble climatology. (b) Annual LIG-PI precipitation anomaly (%ΔP) for the full ensemble subset of the three models that agree most closely with the LIG proxy network. (c) Heat map same as in Figure 2 for LIG-PI, including AC2 values for the full PMIP4 ensemble and ensembles of the top two, three, four, and five models in terms of agreement with the LIG proxy network. (d - f) Same as Figure 2 for three models in the ensemble in b. (d: NESM3, e: INM-CM4-8, f: CNRM-CM6). Dark gray dashed and light gray dotted lines same as in Figure 2.

3.4 Last Interglacial proxy network – model comparisons

Agreement between the proxy network and model simulations is greater for the LIG than for the MH for both precipitation (Figure 3c) and effective moisture (Supplement XX). The LIG ensemble (n = 15) produces an AC2 value of 0.46 at an intermediate rainfall threshold of 12% (Figure 3a), which is a higher degree of agreement than 13 of the 15 individual models (Figure

3c). The model NESM3 produces the highest degree of agreement with the proxy network, with an AC2 value of 0.64 at a rainfall threshold of 1, 2, or 3% (Figure 3d). The models INM-CM4-8 (Figure 3e) and CNRM-CM6 (Figure 3f) display the second and third highest values, 0.51 and 0.44 respectively, at rainfall thresholds of 2%. Most other models are optimized at rainfall thresholds between 12% and 20% and display AC2 values that range from 0.21 to 0.43 (Figure 3c). MIROC-ES2L and FGOALS-g3 are the only two models with middling AC2 values (0.38 and 0.37 respectively) that are optimized at rainfall thresholds of less than 2%. The four models with AC2 values of less than 0.25 are not considered statistically significant comparisons ($p > 0.05$).

Increased rainfall in Alaska and the southwest US, where LIG proxies indicate wetter conditions, is relatively consistent across all models and is represented by robust wetness (>12% rainfall anomaly) in the ensemble (Figure 3). Most models and the ensemble also show a domain of increased LIG aridity in the northern Great Plains, though there are no LIG proxy sites in this region for comparison. There is significant disagreement in the sign of rainfall change between models across most of the rest of North America, though the magnitude of anomaly tends to be smaller than in the southwest US or northern Great Plains. The LIG ensemble is characterized by a transition between wetness in the west and aridity in the Midwest and east that runs from southeastern New Mexico through Idaho, though the magnitude of anomaly across these regions is below the optimized rainfall threshold of 12%. This pattern drives weak disagreement with the drier proxy records distributed across the Pacific Northwest and Rocky Mountain region and with the wetter records of southern Illinois, the Gulf of Mexico, and the coastal southeast US.

K_w values are lower than AC2 values for all LIG simulations, as are AC1 values, though to a lesser degree. The same four models perform the best across all three metrics except for FGOALS-g3, which improves from eighth highest AC2 to second highest K_w and fourth highest AC1. K_w values less than 0.2 (10 models) and AC1 values less than 0.22 (9 models) are statistically nonsignificant results ($p > 0.05$) (Table S4). As with the MH, we focus our discussion on LIG AC2 values.

4 Discussion

4.1 Mid-Holocene comparisons and climate interpretations

Our findings are consistent with previous analyses of PMIP simulations which found that models produce opposite sign and/or smaller magnitude MH precipitation anomalies in North America than are suggested by paleoclimate proxy reconstructions (Braconnot et al., 2012; Harrison et al., 2015, 2016; Hermann et al., 2018). Like Hermann et al. (2018), overall agreement between the expanded North American proxy network and MH simulations is low and FGOALS-g3 displays the highest degree of agreement. This agreement appears to be largely driven by widespread MH dry anomalies in western North America present in both FGOALS-g2 (Hermann et al., 2018) and FGOALS-g3 (this study) simulations, where there is a high concentration of proxies that indicate aridity.

The fact that the calculated AC2 values for our new expanded proxy network (Table S3) and for the western US proxy network from Hermann et al. (2018) (Table S5) tend to be higher overall than the K_w values from Hermann et al. (2018) is likely because K_w may be an unreliable metric in cases where agreement is high and there is a large prevalence of one category (Wongparakan et al., 2013; Gwet, 2008; Gwet, 2015). This is the case for comparisons between model simulations and the MH proxy network, which is skewed toward drier conditions and likely explains why the K_w values for the expanded MH proxy network of this study are lower than the AC2 values. Thus, we identify Gwet's AC2 as a more reliable metric for comparisons between climate model output and categorical proxy data and recommend its use for these types of analyses (cf. Feng et al., 2022). However, we do not interpret our higher AC2 values for the expanded network relative to the K_w values for the western US from Hermann et al. (2018) as necessarily indicative of a meaningful improvement on proxy network-model agreement for the MH since this finding is at least partly an artifact of the metrics themselves.

In most cases, our algorithm for choosing a MH precipitation threshold to optimize AC2 results in large thresholds, widespread weak disagreement with any proxy site that is coded as wetter or drier, and a clustering of AC2 values between 0.19 and 0.23. This makes it difficult to differentiate between models in terms of agreement with our expanded proxy network, despite considerable variability in the pattern of precipitation anomalies across North America between model simulations. It is possible that MH proxies are responding in a non-linear way, recording signals of increased aridity in response to small changes in actual rainfall, or are being interpreted here and in past literature as annual signals when they are in fact biased toward anomalies present only in particular seasons.

Alternatively, the MH hydroclimate patterns suggested by the proxy network may be largely driven by climate feedbacks, such as vegetation shifts, that are not fully represented in the model simulations. Changes in vegetation can influence climate via changes to water cycling, surface albedo, and dust mobilization (Thompson et al., 2022) and can drive different dynamical circulation patterns than those expected from orbital, greenhouse gas, and ice sheet forcing alone (Swann et al. 2014). Since the differences in orbital forcing and other CMIP6/PMIP4 boundary conditions between the MH and PI are relatively small, especially compared to those of the LIG, these finer-scale emergent climate feedbacks, such as vegetation response to seasonally biased MH warming, may be especially important for the precipitation dynamics of the MH. None of the MH simulations include fully dynamic vegetation and the few that include interactive vegetation do not stand out in the quality of comparison with the MH proxy network (Table S3). Recent modeling efforts with varying prescriptions for vegetation in the African Sahara, NH mid-latitudes, and Arctic have yielded improved agreement with temperature estimates from the Temperature12K database (Kaufman et al., 2020) during the Holocene (Thompson et al. 2022). Further, vegetation feedbacks during the MH such as a Green Sahara (Tabor et al. 2020) or expanded Eurasian forest cover (Swann et al. 2014) have been shown to help resolve mismatches between simulated and observed precipitation response on a global scale. While dynamical treatment of vegetation remains a challenge for Earth system models of past and present climates, it may contribute to the mismatch between our North American proxy network and the CMIP6/PMIP4 simulations. Additionally, despite the higher resolution of the CMIP6/PMIP4 simulations, they appear not to have improved in terms of the simulation of extratropical circulation relative to CMIP5/PMIP3 (Brierley et al., 2019), an issue that has been pinpointed as a likely cause of mismatches between simulated and observed moisture patterns in Eurasia (Bartlein et al., 2017) and Europe (Mauri et al., 2014) and one that may play an important role for North America as well. The persistent mismatch between the modest MH rainfall anomalies of PMIP simulations and the patterns evident in MH proxy networks deserves further consideration.

4.2 Last Interglacial comparisons and climate interpretations

Our LIG analyses expand upon previous work by Scussolini et al. (2019), whose comparisons show agreement between their proxy network and model ensemble (n = 7) on increased LIG rainfall in Alaska and northern South America, but an ambiguous relationship across the contiguous US. Similarly, we observe weak disagreement between our LIG ensemble (n = 15) and expanded LIG proxy network in much of the US (Figure 3a).

We find that an ensemble of the three models that most closely agree with the LIG proxy network and are optimized at a relatively low rainfall threshold of 2% – NESM3, INM-CM4-8, and CNRM-CM6 – maximizes agreement with the LIG proxy network relative to any other individual model or combination of models (Figure 3b). This subset ensemble displays an AC2 value of 0.66 at an optimized rainfall threshold of 1%. Agreement with the wetter proxy sites in Alaska and southern California is consistent between the subset ensemble (n = 3) and full ensemble (n = 15). However, the subset ensemble shows better agreement with drier proxy sites in the Pacific Northwest and in the Rocky Mountains, where it displays low magnitude, but robust dry anomalies. The low magnitude wet anomalies in the full ensemble are below the optimized rainfall threshold, driving weak disagreement with all but the Porcupine Creek record of western Wyoming which has been interpreted as representing moisture conditions similar to the present day (Pierce et al., 2011). The subset also aligns more closely with the wetter proxy sites of southern Illinois in the Midwest US and of the Gulf of Mexico and the coastal southeast US, all of which are situated close to the wet-dry anomaly transition, likely contributing to the low optimized rainfall threshold of the subset ensemble. Thus, our subset ensemble may help reconcile disagreement between the aridity in the Mississippi River Basin of the full LIG ensemble and LIG proxies in southern Illinois, which indicate enhanced LIG rainfall. Finally, the subset shows a wetter southern Caribbean, where three of the five records in our compilation are wetter, compared to the ambiguous climatology of the full ensemble.

4.3 Last Interglacial seasonal considerations

Individual PMIP4 simulations display variable responses to the enhanced seasonality that was driven by the orbital forcing of the LIG. We avoid quantitative comparisons between models and proxies on a seasonal basis because robust seasonal biases in LIG proxy records are often unclear, speculative, or in development in the paleoclimate proxy literature (Kwiacien et al., 2022 and references therein). Instead, we compare the subset of models that maximize annual agreement with the LIG proxy network (Figure 4c, d) with the full PMIP4 ensemble (Figure 4a, b) to help elucidate some of the seasonal patterns in North American LIG rainfall. During the LIG summer half-year (MJJASO) both the full ensemble and the ensemble subset are characterized by wetter conditions across Alaska, northern Canada, and Mexico and drier conditions in southern Canada, the central US, and the Pacific Northwest (Figure 4a, c). Both show enhanced aridity in eastern Canada, the northern Great Plains, and northeast US and wetter conditions in the southwestern US and Mexico during the winter half-year (NDJFMA) (Figure 4b, d).

During the winter half-year (NDJFMA) the subset ensemble shows increased rainfall in the southeastern US, where the full ensemble indicates aridity, and a mix of wet and dry conditions along the northwest coast of the US and Canada, where the full ensemble shows contiguous wetness (Figure 4b, d). The subset ensemble displays more widespread wet conditions in the eastern US and in northern South America during the summer half-year relative to the full ensemble (Figure 4a, c).

Additionally, the subset ensemble differs from the full ensemble in terms of the seasonal pattern of wet anomalies in the North American Monsoon (NAM) region. While many models show a positive annual rainfall anomaly in the southwestern US, a closer look at the spatial distribution and seasonal balance of rainfall between models indicates that different mechanisms drive this annual anomaly in each model (Figure 4). The annual increase in rainfall in the southern US may result from an expanded and strengthened NAM, a strengthened, but not significantly expanded monsoon, or an increase in southwesterly winter rainfall. Scussolini et al. (2019) observe a wetter and somewhat spatially expanded LIG NAM in their ensemble climatology, though there is considerable inter-model spread that hinders a more conclusive understanding of how far into California and/or the Great Basin this anomaly extends. Similarly, our full ensemble shows enhanced summer half-year rainfall occurring from southern California into the southern Great Basin and as far east as central New Mexico (Figure 4a). The subset ensemble differs from the full ensemble in that it is characterized by a summer half-year rainfall anomaly that extends northward from Mexico but is localized to Arizona within the United States and does not extend west to the wetter LIG proxies of southern California (Figure 4c). Taken individually, there is disagreement among the top three models in the spatial distribution of summer moisture in the southwestern United States. NESM3 shows enhanced rainfall across Mexico and into Arizona and New Mexico (Figure 4e). INM-CM4-8 displays an opposite response, showing enhanced summer aridity across the NAM domain, including northern and central Mexico (Figure 4g). CNRM-CM6 shows greatly enhanced rainfall in southern California and Arizona that extends northward into southern Nevada (Figure 4i). A lack of resolvable proxies in northern Mexico, Arizona, and New Mexico, as well as the southern Rockies, makes specific interpretations about the geometry of the NAM domain during the LIG challenging. The development of new proxy records from these climatologically important but currently unrepresented locations will be key for generating a better understanding of the characteristics of regional precipitation patterns during the LIG, like the NAM.

The top three models are in much closer agreement with regard to cool season rainfall, with all three showing enhanced wetness across the southwest US during the winter half-year (Figure 4f, h, j). Thus, a key finding of this work is that this subset of models indicates that the NAM may have been strengthened, but perhaps not significantly expanded during the LIG and that the enhanced annual wetness of the southwestern US, including that which is demonstrated by the southern California proxies, was driven primarily by increased southwesterly wintertime rainfall not summertime monsoonal rainfall.

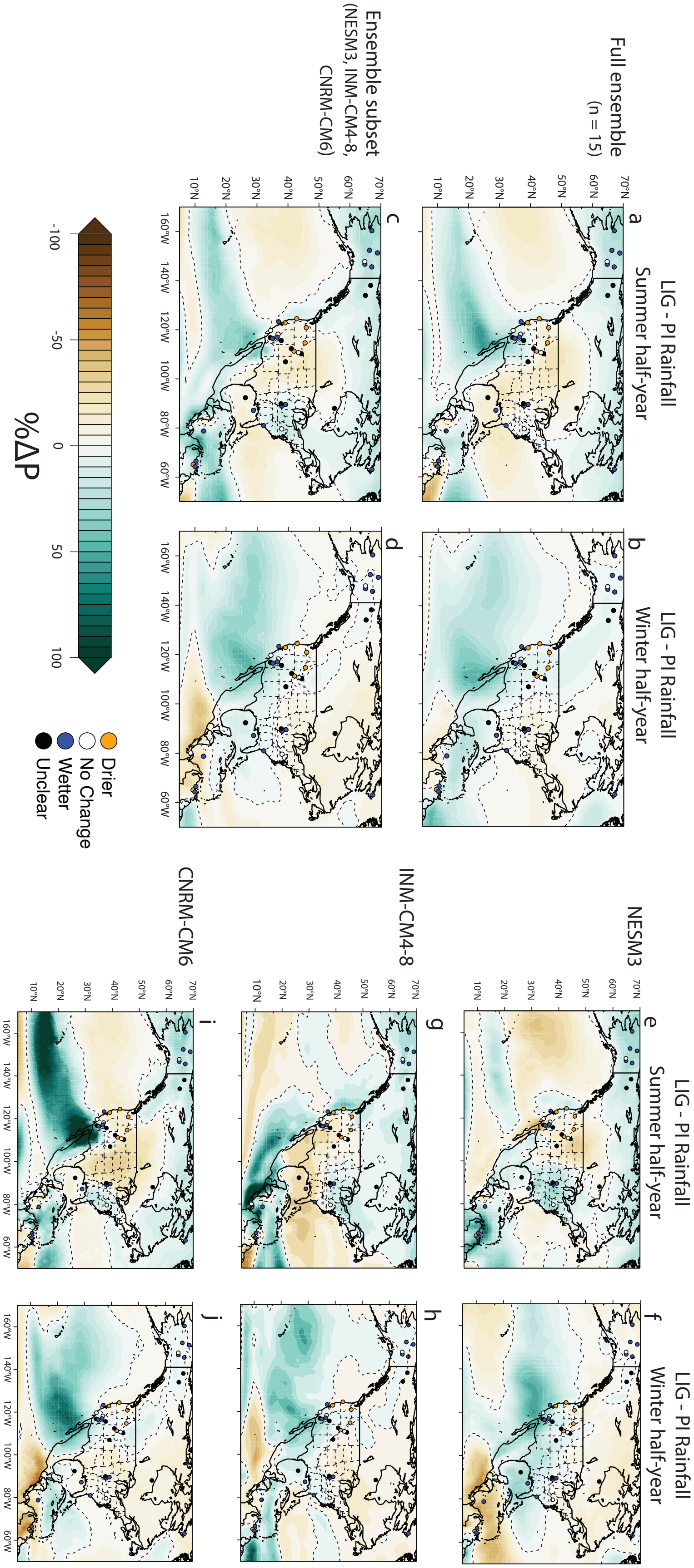
Full ensemble
(n = 15)
Ensemble subset
(NESM3, INM-CM4-8,
CNRM-CM6)
LIG - PI Rainfall
Summer half-year
LIG - PI Rainfall
Winter half-year
NESM3
INM-CM4-8
CNRM-CM6
a
b
c
d
e
f
g
h
i
j
70°N
60°N
50°N
40°N
30°N
20°N
10°N
160°W
140°W
120°W
100°W
80°W
60°W
-100
-50
0
50
100
%ΔP
Drier
No Change
Wetter
Unclear

Figure 4. Summer (MJJASO) and winter (NDJFMA) half-year LIG - PI rainfall anomalies for the full PMIP4 ensemble (a and b), the ensemble subset (c and d), and the three models that make up the ensemble subset (NESM3: e and f; INM-CM4-8: g and h; CNRM-CM6: i and j). Proxy sites are plotted based on rainfall designation at the LIG relative to the PI. Dark gray dashed lines and light gray dotted lines same as in Figure 2.

4.4 Atmospheric dynamics during the Last Interglacial

To assess the atmospheric drivers of LIG moisture patterns, we present sea level pressure (SLP) and 850 hPa wind vector output for the ensemble of the three models that agree most closely with the LIG proxy record (Figure 5). Interactions between the semi-permanent pressure systems over the Pacific and Atlantic play a large role in the amount and seasonal distribution of rainfall that falls across much of North America (e.g., Wise, 2016). Specifically, the location and relative strength of the North Pacific High (NPH) and Aleutian Low (AL) are relevant for the geometry of winter storm tracks that deliver moisture to Alaska and the western US, where there is a large concentration of LIG proxy sites (e.g., Oster et al., 2015; Wong et al., 2016; Swain, 2015). In the eastern US, the gradient between low SLP in the subtropical Atlantic Ocean and high SLP in the north Atlantic and the position of the North Atlantic Subtropical High (NASH) and has been shown to play a large role in the amount and source of rainfall during both the modern (Labosier and Quiring, 2013; Diem, 2012; Li et al., 2011) and the Holocene (Hardt et al., 2010), including via the incidence of summer tropical cyclones along the Gulf Coast and east coast of North America (e.g., Baldini et al., 2016). An assessment of how these pressure systems differed under the enhanced seasonality of the LIG relative to the PI may thus provide insights into the mechanisms driving the spatial patterns and seasonal distribution of LIG rainfall.

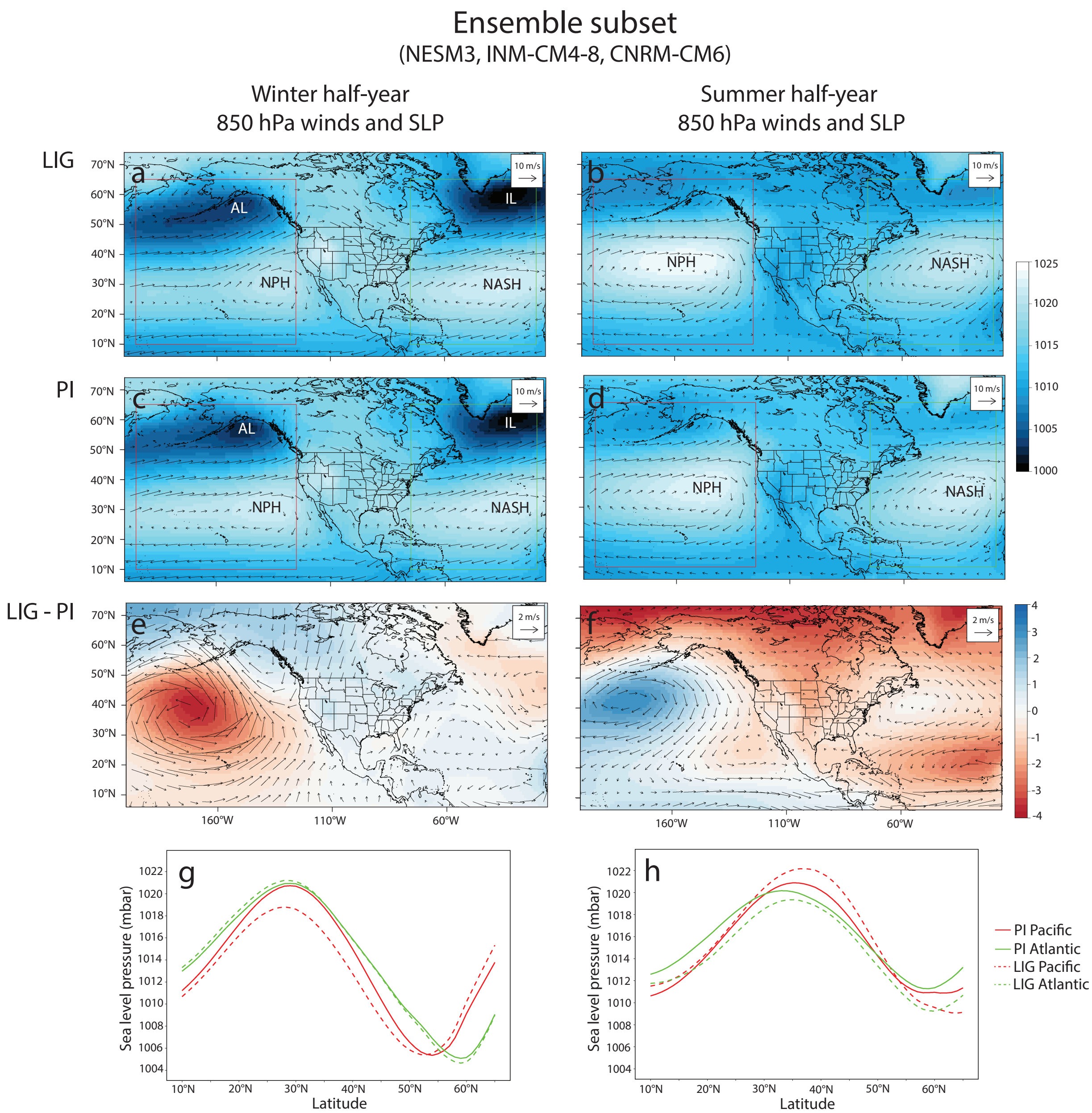

Figure 5. Ensemble subset summer half-year and winter half-year 850 hPa wind vectors and sea level pressure for the LIG (a, b), PI (c, d), and LIG-PI anomaly (e, f). Latitudinal pressure gradient for 10°N to 65°N zonally averaged from 165°W to 235°W in the Pacific Ocean (red box in a-d) and from 75°W to 20°W in the Atlantic Ocean (green box in a-d) for the LIG and PI. AL: Aleutian Low. NPH: North Pacific High. IL: Icelandic Low. NASH: North Atlantic Subtropical High.

During the winter half-year, the LIG NPH is weaker and less longitudinally expansive, and the AL is less deep in the Gulf of Alaska but extends further west along the Aleutian Island chain relative to the PI (Figure 5a, c, e). Correspondingly, the gradient between the AL and NPH is weaker during the LIG winter (Figure 5g), as illustrated by the large negative winter SLP pressure anomaly in the central Pacific between 20 and 50°N and the associated strong cyclonic surface wind vector anomalies (Figure 5e).

In the southwestern US, where enhanced rainfall is shown in the ensemble subset and by the proxy records, the slackened LIG SLP gradient in the Pacific may have allowed for more westerly storms to penetrate the continent, driving fewer large-scale droughts and the overall wetter winter half-year conditions relative to the PI. This pressure configuration is largely inverse that which characterized western US-wide droughts over the last 500 years (Wise 2016). These dry intervals are characterized by a strong AL, anomalously low pressure over eastern North America, and an intense high-pressure ridge centered over the Pacific Northwest, which would block storms from penetrating into the Western US and enable prolonged dry conditions. The model simulations indicate that these pressure conditions may have been less pervasive on average during the LIG winters, which could explain the enhanced southwestern US wetness simulated by the models and shown by proxy records.

The ensemble subset winter half-year moisture signal is less clear in northwestern NA, with low magnitude wet anomalies in eastern Alaska and low magnitude dry anomalies in British Columbia (Figure 4d). The weaker and westerly expanded AL and northerly wind vector anomalies in the eastern Gulf of Alaska during the LIG (Figure 5e) are characteristic of a neutral-to-strong negative Pacific Decadal Oscillation/positive North Pacific Index (-PDO/+NPI) phase (Anderson et al., 2016). However, the relationship between the strength of the AL and high latitude hydroclimate is complicated and the longitudinal position of the AL center during -PDO/+NPI states can be highly variable (Rodionov et al., 2007; Anderson et al., 2016). So, while we do observe a difference in the AL geometry between the LIG and PI that has implications for PDO/NPI dominance, given the small magnitude of the LIG winter rainfall anomalies in Alaska and western Canada, the importance of the strength and position of the AL for LIG high latitude hydroclimate is somewhat ambiguous.

During the winter half-year, the ensemble subset LIG SLP anomalies in the Gulf of Mexico and Atlantic Ocean are lower magnitude than those of the Pacific Ocean. We observe slightly higher LIG subtropical Atlantic SLPs and lower LIG SLPs in the northern Atlantic (Figure 5e) driving a moderate strengthening of the LIG latitudinal SLP gradient (Figure 5g). This configuration may indicate a slight preference for a more positive North Atlantic Oscillation (+NAO), which is associated with a steepening of the longitudinal Atlantic SLP gradient (Hurrell, 1995) and an enhancement of westerly flow (Rogers, 1990), during the LIG. A slight negative correlation exists between NAO and total winter precipitation in New England (e.g., Ning and Bradley, 2015) and other parts of the northeastern US (e.g. Morin et al., 2008), where the ensemble subset produces dry winter half-year rainfall anomalies during the LIG. The dry LIG anomalies extend throughout most of Canada in the ensemble subset winter half-year, but the correlation between NAO and modern total winter precipitation is less clear in eastern Canada (Bonsal and Shabbar, 2008; Chartrand and Pausata, 2020).

In the southeast US, the ensemble subset displays moderate northeasterly wind vector anomalies during the LIG winter half-year in the Gulf of Mexico and extending into Florida (Figure 5e). This may contribute to the wet anomalies across the southeast US during the winter half-year observed in the subset ensemble (Figure 4d), and is consistent with observations of increased fall rainfall in the region during the 20th-century (Bishop et al. 2018).

During the LIG summer half-year the model simulations produce a stronger and more expansive NPH and lower SLPs across Alaska, Canada, and most of the contiguous US relative to the PI (Figure 5b, d, f). This results in a steeper LIG latitudinal pressure gradient (Figure 5h) and strong anticyclonic surface wind vector anomalies in the north Pacific relative to the PI (Figure 5f), which may have facilitated greater delivery of oceanic moisture to the Alaska interior and western Canada, where the ensemble subset indicates enhanced wetness (Figure 4c). The wet LIG anomalies do not extend past the west coast of the US, which may be related to the westward expansion of the NPH and the corresponding enhancement of southward meridional wind vector anomalies in the east Pacific that do not penetrate the continental interior.

The Atlantic Ocean is characterized by negative pressure anomalies in the subtropics and high latitudes (>50°N) during the LIG summer half-year relative to the PI (Figure 5f) and a LIG SLP gradient that is shifted northward and lower in magnitude than that of the PI (Figure 5h). The subtropical negative anomalies indicate a weakening of the NASH during the LIG, especially in the eastern Atlantic where the anomalies are largest (Figure 5f). A weakened and northward shifted NASH is associated with the warm phase of the Atlantic Meridional Oscillation (+AMO), which has been shown to drive decreased modern rainfall across the central US via diminished advection of moist, maritime air into the continental interior (Hu et al., 2011). A preference for a +AMO phase during the LIG is consistent with the dry summer half-year anomalies in the central US in the ensemble subset (Figure 4c). The warm phase of the AMO is also associated with enhanced easterly and northeasterly flow onshore flow to the southeastern US and increased summertime rainfall (Hu et al., 2011), which is reflected in the ensemble subset summer half-year easterly wind vector anomalies (Figure 5f) and positive rainfall anomalies (Figure 4c). Florida is the exception in that it is drier in the LIG ensemble subset. This may be related to the displacement of the tropical easterlies that flow south of the NASH, which leads to diminished advection of moist, unstable air to Florida and drier conditions (Coleman, 1988, Labosier and Quiring, 2013). This matches the pattern of summer half-year aridity in Florida and the Gulf of Mexico in the ensemble subset (Figure 4c) and the splitting of easterly wind vector anomalies to the north and south around Florida (Figure 5f).

Importantly, local thermodynamic forcing may also contribute to greater LIG rainfall through intensification of the hydrologic cycle (Huntington et al., 2018), especially in the northern latitudes where the enhanced seasonality of the LIG drove the largest degree of summer warming. While the clearest influence of warming on the hydrologic cycle is likely increased evaporative demand (Dai et al., 2018), it may also drive an intensification of major oceanic moisture sources for continental precipitation, especially for North America (Gimeno et al., 2013), and contribute to the observed and simulated LIG precipitation patterns.

5 Conclusions: The Last Interglacial as an analog for future moisture patterns

We present comparisons between updated MH and LIG moisture-sensitive proxy networks and model output from the latest generation of PMIP simulations to assess agreement between the two during the two most recent intervals when NH temperatures were warmer than the PI.

We find low overall agreement between our new and expanded MH proxy network and PMIP4 MH simulations, with most models producing the opposite sign and/or smaller magnitude

MH precipitation anomalies than demonstrated by the proxy network. These findings are consistent with previous comparisons between PMIP simulations and North American moisture-sensitive proxy records (Braconnot et al. 2012; Harrison et al. 2015, 2016; Hermann et al. 2018) and point toward the presence of unconstrained biases or non-linearities in the proxy records and/or the importance of climate feedbacks that are not fully represented in model simulations for NA hydroclimate during the MH.

Agreement between our LIG proxy network and PMIP4 simulations is higher than for the MH and we find that an ensemble subset of the three models that agree most closely with the proxy network generates the highest AC2 value overall. The ensemble subset helps reconcile differences between the simulated precipitation anomalies of the full PMIP4 ensemble and the LIG proxy network in the Pacific Northwest, Rocky Mountains, northern Mississippi River Basin, and coastal southeastern US. We then use this ensemble subset to assess the seasonal patterns of LIG precipitation, with a key finding being that the NAM may have been strengthened, but not significantly expanded northward during the LIG, and that the wet anomalies of southern California LIG proxy records were primarily driven by increased southwesterly wintertime rainfall, as opposed to summertime monsoonal rainfall.

We find that shifts in the semi-permanent pressure systems in the Atlantic and Pacific during the LIG may have impacted the amount and seasonal distribution of precipitation in much of North America. Specifically, we observe a weakening of the winter half-year LIG latitudinal SLP gradient in the Pacific and a strengthening and northward displacement of the summer half-year LIG Pacific and Atlantic SLP gradients, with important implications for moisture transport and the seasonal and spatial distribution of simulated LIG precipitation anomalies across North America.

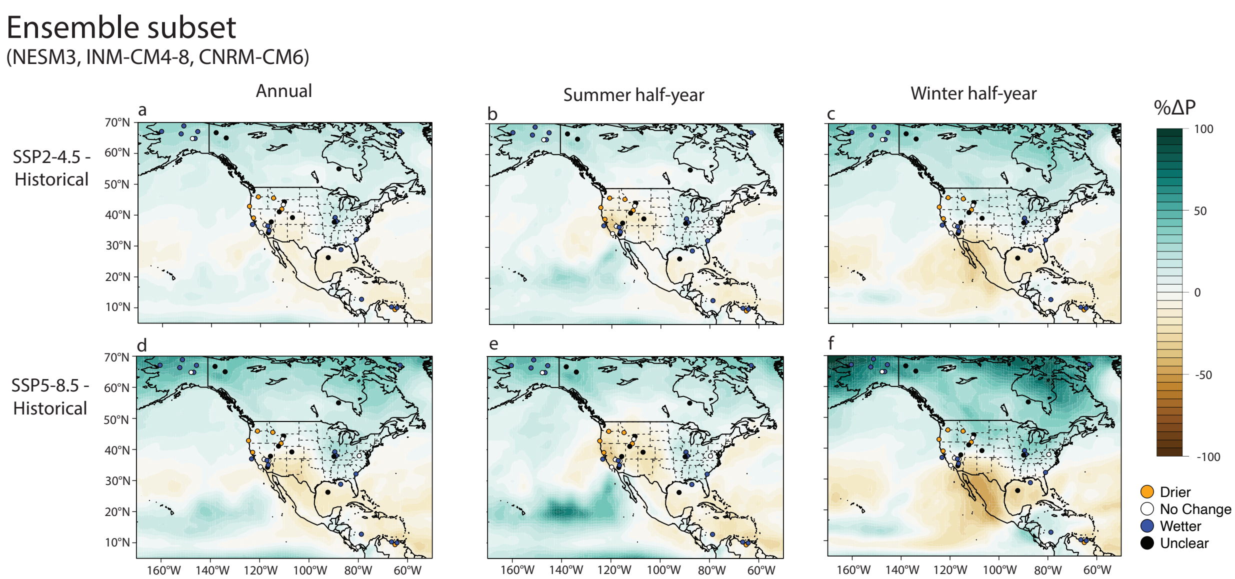

Figure 6. Annual, summer (MJJASO) and winter half-year (NDJFMA) precipitation anomalies (% change, 2071-2100 versus 1850-1949) for the SSP2-4.5 (a-c) and SSP5-8.5 (d-f) simulations in the ensemble subset. LIG proxy sites are plotted based on moisture designation for comparison with projected rainfall patterns.

Comparisons between climate model simulations and proxy data from forcing scenarios that are outside the bounds of the preindustrial or historical period are critical for the evaluation of the newest generation of models (Tierney et al. 2020). However, the utility of using large ensembles of past and future climate model simulations can be limited at times because a lack of robust agreement between different models produces inconclusive results across key regions (e.g., Scussolini et al. 2019; Cook et al. 2020). Our approach may aid in navigating around this problem by providing a rationale to consider a particular subset of models based on the degree of agreement with proxy records for past time periods. Given that the LIG has been proposed as an analog for low end later 21st century radiative forcing scenarios (Burke et al., 2018), the subset of models that agree most closely with the LIG proxy network may provide more informative projections of near-future precipitation patterns relative to the full ensemble. To conclude, we evaluate our subset from the framework of both comparison with the LIG proxies and for relevancy for future hydroclimate projections.

We present precipitation anomalies between the 'historical' (1850-2014) simulations and two SSP (2015-2100) scenarios – SSP2-4.5 (+4.5 W m^{-2}; medium forcing pathway) and SSP5-8.5 (+8.5 W m^{-2}; high-end forcing pathway) for our ensemble subset that maximizes agreement with the LIG proxy record (Figure 6). On an annual basis the ensemble subset predicts increased precipitation across Alaska, Canada, the Pacific Northwest, the Great Lakes region, and the eastern US and decreased precipitation in Mexico, Texas, and the southwestern US for the SSP2-4.5 scenario (Figure 6a-c). Greater magnitude changes in the same spatial pattern are projected for the SSP5-8.5 scenario in the subset ensemble (Figure 6d-f). These findings are largely consistent with those from the model ensemble (n=13) produced by Cook et al. (2020) who observe robust wetting in Alaska, Canada, and the eastern US and drying in western and southern Mexico and Central America, but non-robust changes in the central and western US.

During the summer half-year, our ensemble subset predicts relatively more arid conditions across the already water-sensitive western US in the SSP2-4.5 simulations (Figure 6b). During the winter half-year arid conditions in the ensemble subset are projected in Mexico and extending northward into Texas, Arizona, New Mexico, and southern California (Figure 6c). The magnitude of these patterns is even greater for the SSP5-8.5 simulation (Figure 6e, f). Outside of these regions the ensemble subset shows mostly positive North American rainfall anomalies, especially in the higher latitudes (Figure 6b, c, e, f).

Qualitative comparisons between our LIG proxy network and the subset ensembles yield mixed results. Annual moisture patterns in the subset ensemble align with LIG proxy signals in some regions for the SSP2-4.5 and SSP5-8.5 simulations, like Alaska and the Midwest US where there are persistent wet anomalies on both the annual and seasonal scale relative to the historical (Figure 6). However, in other regions the alignment between the LIG proxy signals and moisture pattern predicted by the SSP simulations are more ambiguous. This includes the concentration of wet and no change proxy records in southern California and the dry proxy sites in the Pacific Northwest, where the SSP5-8.5 ensemble subsets point to enhanced aridity across both seasonal half-years (Figure 6d, e, f). The SSP2-4.5 ensemble subset is more equivocal, which is expected given the smaller overall anthropogenic forcing, but still tends drier in this region (Figure 6a, b, c). The projected annual wetness of the Pacific Northwest and Northern Rockies for the future scenarios does not align with the aridity indicated by the LIG proxies in these regions (Figure 6a, d), though this comparison is complicated by the fact that summer half-years are projected to be drier under both the SSP2-4.5 and SSP5-8.5 scenarios (Figure 6b, e). This points to the difficulty of carrying out comparisons on a seasonal basis without a robust understanding of seasonal biases in the proxy records.

Ultimately, the differences between the orbitally controlled radiative forcing of the LIG and the enhanced greenhouse effect of the end 21st century could mean that alignment between the moisture patterns of the LIG and SSP simulations is coincidental. It may be the case that other climate states from deeper time, like the Pliocene or Eocene, provide closer analogs for near future warming (Burke et al., 2018). Even so, our quantitative comparisons between an updated and expanded LIG proxy network and the newest generation of PMIP simulations can aid in the evaluation of the Earth system models that we rely on for projecting future climate states that are beyond the range of the preindustrial or historical records that models are often tuned to (Tierney et al., 2020).

6 Acknowledgements

This work was supported by NSF grants AGS-1203701, AGS-1554998, and AGS-2102884 to J.L.O; and AGS-2102901 to D.E.I. We thank the modeling groups for archiving results through the CMIP5 Data Portal (https://esgf-node.llnl.gov/search/cmip6/). All data used in model–proxy comparisons are available in the supporting information and are available for download from the NOAA National Climatic Data Center's Paleoclimatology database. R scripts used to process and analyze climate model data and carry out comparisons with proxy networks are available upon from the authors.

References

Adam, D. P., and West, G. J. (1983). Temperature and Precipitation Estimates Through the Last Glacial Cycle from Clear Lake, California, Pollen Data. *Science*, *219*(4581), 168 LP – 170. https://doi.org/10.1126/science.219.4581.168

Anderson, L., Berkelhammer, M., Barron, J. A., Steinman, B. A., Finney, B. P., & Abbott, M. B. (2016). Lake oxygen isotopes as recorders of North American Rocky Mountain hydroclimate: Holocene patterns and variability at multi-decadal to millennial time scales. *Global and Planetary Change*, *137*, 131–148. https://doi.org/https://doi.org/10.1016/j.gloplacha.2015.12.021

Anderson, R. S., Jiménez-Moreno, G., Ager, T., & Porinchu, D. F. (2014). High-elevation paleoenvironmental change during MIS 6–4 in the central Rockies of Colorado as determined from pollen analysis. *Quaternary Research*, *82*(3), 542–552. https://doi.org/DOI: 10.1016/j.yqres.2014.03.005

Baker, R. G. (1986). Sangamonian(?) and Wisconsinan paleoenvironments in Yellowstone National Park. *GSA Bulletin*, *97*(6), 717–736. https://doi.org/10.1130/0016-7606(1986)97<717:SAWPIY>2.0.CO;2

Balch, D. P., Cohen, A. S., Schnurrenberger, D. W., Haskell, B. J., Valero Garces, B. L., Beck, J. W., Cheng, H., & Edwards, R. L. (2005). Ecosystem and paleohydrological response to Quaternary climate change in the Bonneville Basin, Utah. *Palaeogeography,* *Palaeoclimatology, Palaeoecology*, *221*(1), 99–122. https://doi.org/https://doi.org/10.1016/j.palaeo.2005.01.013

Baldini, L. M., Baldini, J. U. L., McElwaine, J. N., Frappier, A. B., Asmerom, Y., Liu, K., Prufer, K. M., Ridley, H. E., Polyak, V., Kennett, D. J., Macpherson, C. G., Aquino, V. V, Awe, J., & Breitenbach, S. F. M. (2016). Persistent northward North Atlantic tropical cyclone track migration over the past five centuries. *Scientific Reports*, *6*(1), 37522. https://doi.org/10.1038/srep37522

Bartlein, P. J., Anderson, K. H., Anderson, P. M., Edwards, M. E., Mock, C. J., Thompson, R. S., Webb, R. S., Webb III, T., & Whitlock, C. (1998). Paleoclimate simulations for North America over the past 21,000 years: features of the simulated climate and comparisons with paleoenvironmental data. *Quaternary Science Reviews*, *17*(6), 549–585. https://doi.org/https://doi.org/10.1016/S0277-3791(98)00012-2

Bartlein, P. J., Harrison, S. P., & Izumi, K. (2017). Underlying causes of Eurasian midcontinental aridity in simulations of mid-Holocene climate. *Geophysical Research Letters*, *44*(17), 9020–9028. https://doi.org/https://doi.org/10.1002/2017GL074476

Bigelow, N. H., Edwards, M. E., Elias, S. A., Hamilton, T. D., & Schweger, C. E. (2014). Tundra and boreal forest of interior Alaska during terminal MIS 6 and MIS 5e. *Vegetation History and Archaeobotany*, *23*(3), 177–193. https://doi.org/10.1007/s00334-013-0425-z

Bishop, D. A., Williams, A. P., Seager, R., Fiore, A. M., Cook, B. I., Mankin, J. S., Singh, D., Smerdon, J. E., & Rao, M. P. (2018). Investigating the causes of increased 20(th)-century fall precipitation over the southeastern United States. *Journal of Climate*, *32*(2), 575–590. https://doi.org/10.1175/JCLI-D-18-0244.1

Bonsal, B., & Shabbar, A. (2008). Impacts of Large-Scale Circulation Variability on Low Streamflows over Canada: A Review. *Canadian Water Resources Journal / Revue Canadienne Des Ressources Hydriques*, *33*(2), 137–154. https://doi.org/10.4296/cwrj3302137

Braconnot, P., Harrison, S. P., Kageyama, M., Bartlein, P. J., Masson-Delmotte, V., Abe-Ouchi, A., Otto-Bliesner, B., & Zhao, Y. (2012). Evaluation of climate models using palaeoclimatic data. *Nature Climate Change*, *2*(6), 417–424. https://doi.org/10.1038/nclimate1456

Brewer, S., Guiot, J., Sánchez-Goñi, M. F., & Klotz, S. (2008). The climate in Europe during the Eemian: a multi-method approach using pollen data. *Quaternary Science Reviews*, *27*(25), 2303–2315. https://doi.org/https://doi.org/10.1016/j.quascirev.2008.08.029

Brierley, C. M., Zhao, A., Harrison, S. P., Braconnot, P., Williams, C. J. R., Thornalley, D. J. R., Shi, X., Peterschmitt, J.-Y., Ohgaito, R., Kaufman, D. S., Kageyama, M., Hargreaves, J. C., Erb, M. P., Emile-Geay, J., D'Agostino, R., Chandan, D., Carré, M., Bartlein, P. J., Zheng, W., … Abe-Ouchi, A. (2020). Large-scale features and evaluation of the PMIP4-CMIP6 \textit{midHolocene} simulations. *Climate of the Past*, *16*(5), 1847–1872. https://doi.org/10.5194/cp-16-1847-2020

Burke, K. D., Williams, J. W., Chandler, M., Haywood, A., Lunt, D., & Otto-Bliesner, B. (2018). Pliocene and Eocene provide best analogs for near-future climates. *Proceedings of the National Academy of Sciences*, *115*, 13288–13293.

Cárdenes-Sandí, G. M., Shadik, C. R., Correa-Metrio, A., Gosling, W. D., Cheddadi, R., & Bush, M. B. (2019). Central American climate and microrefugia: A view from the last interglacial. *Quaternary Science Reviews*, *205*, 224–233. https://doi.org/https://doi.org/10.1016/j.quascirev.2018.12.021

Chartrand, J., & Pausata, F. S. R. (2020). Impacts of the North Atlantic Oscillation on winter precipitations and storm track variability in southeast Canada and the northeast United States. *Weather and Climate Dynamics*, *1*(2), 731–744. https://doi.org/10.5194/wcd-1-731-2020
Chartrand, J., & Pausata, F. S. R. (2020). Impacts of the North Atlantic Oscillation on winter precipitations and storm track variability in southeast Canada and the northeast United States. *Weather and Climate Dynamics*, *1*(2), 731–744. https://doi.org/10.5194/wcd-1-731-2020
Coleman, J. (1988). Climatic warming and increased summer aridity in Florida, U.S.A. *Climatic Change*, *12*, 165–178. https://doi.org/10.1007/BF00138937

Conroy, J. L., Karamperidou, C., Grimley, D. A., & Guenthner, W. R. (2019). Surface winds across eastern and midcontinental North America during the Last Glacial Maximum: A new data-model assessment. *Quaternary Science Reviews*, *220*(August), 14–29. https://doi.org/10.1016/j.quascirev.2019.07.003

Consortium, P. H. (2017). Comparing proxy and model estimates of hydroclimate variability and change over the Common Era. *Clim. Past*, *13*(12), 1851–1900. https://doi.org/10.5194/cp-13-1851-2017

Cook, B. I., Mankin, J. S., Marvel, K., Williams, A. P., Smerdon, J. E., & Anchukaitis, K. J. (2020). Twenty-First Century Drought Projections in the CMIP6 Forcing Scenarios. *Earth's Future*, *8*(6), e2019EF001461. https://doi.org/https://doi.org/10.1029/2019EF001461

Curry, B. B., & Baker, R. G. (2000). Palaeohydrology, vegetation, and climate since the late Illinois Episode (∼130 ka) in south-central Illinois. *Palaeogeography, Palaeoclimatology, Palaeoecology*, *155*(1), 59–81. https://doi.org/https://doi.org/10.1016/S0031-0182(99)00094-2

D., B. K., W., W. J., A., C. M., M., H. A., J., L. D., & L., O.-B. B. (2018). Pliocene and Eocene provide best analogs for near-future climates. *Proceedings of the National Academy of Sciences*, *115*(52), 13288–13293. https://doi.org/10.1073/pnas.1809600115

Dai, A., Zhao, T., & Chen, J. (2018). Climate Change and Drought: a Precipitation and Evaporation Perspective. *Current Climate Change Reports*, *4*(3), 301–312. https://doi.org/10.1007/s40641-018-0101-6

Dalmonech, D., Zaehle, S., Schürmann, G., Brovkin, V., Reick, C., & Schnur, R. (2015). Separation of the Effects of Land and Climate Model Errors on Simulated Contemporary Land Carbon Cycle Trends in the MPI Earth System Model version 1*. *Journal of Climate*, *28*, 272–291. https://doi.org/10.1175/JCLI-D-13-00593.1

Delire, C., Levis, S., Bonan, G., Foley, J., Coe, M., & Vavrus, S. (2002). Comparison of the climate simulated by the CCM3 coupled to two different land-surface models. *Climate Dynamics*, *19*(8), 657–669. https://doi.org/10.1007/s00382-002-0255-7

Deposits, P. N., Hudson, I., Lowland, B., & Wyatt, P. H. (1990). Amino Acid Evidence Indicating Two or More Ages of Pre-Holocene Nonglacial Deposits In Hudson Bay Lowland, Northern Ontario. *Géographie Physique et Quaternaire*.

Diem, J. E. (2013). Influences of the Bermuda High and atmospheric moistening on changes in summer rainfall in the Atlanta, Georgia region, USA. *International Journal of Climatology*, *33*(1), 160–172. https://doi.org/https://doi.org/10.1002/joc.3421

Diffenbaugh, N. S., Swain, D. L., & Touma, D. (2015). Anthropogenic warming has increased drought risk in California. *Proceedings of the National Academy of Sciences*, *112*(13), 3931–3936. https://doi.org/10.1073/pnas.1422385112

Feng, R., Bhattacharya, T., Otto-Bliesner, B. L., Brady, E. C., Haywood, A. M., Tindall, J. C., Hunter, S. J., Abe-Ouchi, A., Chan, W. Le, Kageyama, M., Contoux, C., Guo, C., Li, X., Lohmann, G., Stepanek, C., Tan, N., Zhang, Q., Zhang, Z., Han, Z., … Peltier, W. R. (2022). Past terrestrial hydroclimate sensitivity controlled by Earth system feedbacks. *Nature Communications*, *13*(1), 1–11. https://doi.org/10.1038/s41467-022-28814-7

Fischer, H., Meissner, K. J., Mix, A. C., Abram, N. J., Austermann, J., Brovkin, V., Capron, E., Colombaroli, D., Daniau, A. L., Dyez, K. A., Felis, T., Finkelstein, S. A., Jaccard, S. L., McClymont, E. L., Rovere, A., Sutter, J., Wolff, E. W., Affolter, S., Bakker, P., … Zhou, L. (2018). Palaeoclimate constraints on the impact of 2 °c anthropogenic warming and beyond. *Nature Geoscience*, *11*(7), 474–485. https://doi.org/10.1038/s41561-018-0146-0

Forester, R. M., Lowenstein, T. K., & Spencer, R. J. (2005). An ostracode based paleolimnologic and paleohydrologic history of Death Valley: 200 to 0 ka. *GSA Bulletin*, *117*(11–12), 1379–1386. https://doi.org/10.1130/B25637.1

Gavin, D., & Brubaker, L. (2015). *Late Pleistocene and Holocene Environmental Change on the Olympic Peninsula, Washington*. *222*. https://doi.org/10.1007/978-3-319-11014-1

Gimeno, L., Nieto, R., Drumond, A., Castillo, R., & Trigo, R. (2013). Influence of the intensification of the major oceanic moisture sources on continental precipitation. *Geophysical Research Letters*, *40*(7), 1443–1450. https://doi.org/https://doi.org/10.1002/grl.50338

Glover, K. C., MacDonald, G. M., Kirby, M. E., Rhodes, E. J., Stevens, L., Silveira, E., Whitaker, A., & Lydon, S. (2017). Evidence for orbital and North Atlantic climate forcing in alpine Southern California between 125 and 10 ka from multi-proxy analyses of Baldwin Lake. *Quaternary Science Reviews*, *167*, 47–62. https://doi.org/https://doi.org/10.1016/j.quascirev.2017.04.028

Grayson, D. K. (2000). Mammalian responses to Middle Holocene climatic change in the Great Basin of the western United States. *Journal of Biogeography*, *27*(1), 181–192. https://doi.org/https://doi.org/10.1046/j.1365-2699.2000.00383.x

Greve, P., Orlowsky, B., Mueller, B., Sheffield, J., Reichstein, M., & Seneviratne, S. I. (2014). Global assessment of trends in wetting and drying over land. *Nature Geoscience*, *7*(10), 716–721. https://doi.org/10.1038/ngeo2247

Gwet, K. (2015). Testing the Difference of Correlated Agreement Coefficients for Statistical Significance. *Educational and Psychological Measurement*, *76*. https://doi.org/10.1177/0013164415596420

Gwet, K. L. (2008). Computing inter-rater reliability and its variance in the presence of high agreement. *British Journal of Mathematical and Statistical Psychology*, *61*(1), 29–48. https://doi.org/10.1348/000711006X126600

Hardt, B., Rowe, H. D., Springer, G. S., Cheng, H., & Edwards, R. L. (2010). The seasonality of east central North American precipitation based on three coeval Holocene speleothems from southern West Virginia. *Earth and Planetary Science Letters*, *295*(3), 342–348. https://doi.org/https://doi.org/10.1016/j.epsl.2010.04.002

Harrison, S. P., Kutzbach, J.-E., Liu, Z., Bartlein, P. J., Otto-Bliesner, B., Muhs, D., Prentice, I. C., & Thompson, R. S. (2003). Mid-Holocene climates of the Americas: a dynamical response to changed seasonality. *Climate Dynamics*, *20*(7–8), 663–688. https://doi.org/10.1007/s00382-002-0300-6

Hermann, N. W., Oster, J. L., & Ibarra, D. E. (2018). Spatial patterns and driving mechanisms of mid-Holocene hydroclimate in western North America. *Journal of Quaternary Science*, *33*(4), 421–434. https://doi.org/10.1002/jqs.3023

Heusser, L. E. (2000). Rapid oscillations in western North America vegetation and climate during oxygen isotope stage 5 inferred from pollen data from Santa Barbara Basin (Hole 893A). *Palaeogeography, Palaeoclimatology, Palaeoecology*, *161*(3), 407–421. https://doi.org/https://doi.org/10.1016/S0031-0182(00)00096-1

Hu, Q., Feng, S., & Oglesby, R. J. (2011). Variations in North American Summer Precipitation Driven by the Atlantic Multidecadal Oscillation. *Journal of Climate*, *24*(21), 5555–5570. https://doi.org/10.1175/2011JCLI4060.1

Huntington, T. G., Weiskel, P. K., Wolock, D. M., & McCabe, G. J. (2018). A new indicator framework for quantifying the intensity of the terrestrial water cycle. *Journal of Hydrology*, *559*, 361–372. https://doi.org/https://doi.org/10.1016/j.jhydrol.2018.02.048

Hurrell, J. W. (1995). Decadal Trends in the North Atlantic Oscillation. *Science (New York, N.Y.)*, *269*, 676–679. https://doi.org/10.1126/science.269.5224.676

Ibarra, D. E., Oster, J. L., Winnick, M. J., Caves Rugenstein, J. K., Byrne, M. P., & Chamberlain, C. P. (2018). Warm and cold wet states in the western United States during the Pliocene–Pleistocene. *Geology*, *46*(4), 355–358. https://doi.org/10.1130/G39962.1

Jiménez-Moreno, G., Scott Anderson, R., & Fawcett, P. J. (2007). Orbital- and millennial-scale vegetation and climate changes of the past 225ka from Bear Lake, Utah–Idaho (USA). *Quaternary Science Reviews*, *26*(13), 1713–1724. https://doi.org/https://doi.org/10.1016/j.quascirev.2007.05.001

Kaufman, D., McKay, N., Routson, C., Erb, M., Dätwyler, C., Sommer, P. S., Heiri, O., & Davis, B. (2020). Holocene global mean surface temperature, a multi-method reconstruction approach. *Scientific Data*, *7*(1), 201. https://doi.org/10.1038/s41597-020-0530-7

Knight, C., Dorale, J., & Edwards, R. (2006). Stalagmite Records of Interglacial and Glacial Flooding at Crevice Cave, Missouri, USA. *AGU Fall Meeting Abstracts*.

Kwiecien, O., Braun, T., Brunello, C. F., Faulkner, P., Hausmann, N., Helle, G., Hoggarth, J. A., Ionita, M., Jazwa, C. S., Kelmelis, S., Marwan, N., Nava-Fernandez, C., Nehme, C., Opel, T., Oster, J. L., Perşoiu, A., Petrie, C., Prufer, K., Saarni, S. M., … Breitenbach, S. F. M. (2022). What we talk about when we talk about seasonality – A transdisciplinary review. *Earth-Science Reviews*, *225*, 103843. https://doi.org/https://doi.org/10.1016/j.earscirev.2021.103843

Labosier, C. F., & Quiring, S. M. (2013). Hydroclimatology of the southeastern USA. *Climate Research*, *57*(2), 157–171. https://doi.org/10.3354/cr01166

Lapointe, F., Francus, P., Lamoureux, S. F., Vuille, M., Jenny, J. P., Bradley, R. S., & Massa, C. (2017). Influence of North Pacific decadal variability on the western Canadian Arctic over the past 700 years. *Climate of the Past*, *13*(4), 411–420. https://doi.org/10.5194/cp-13-411-2017

Li, W., Li, L., Fu, R., Deng, Y., & Wang, H. (2011). Changes to the North Atlantic Subtropical High and Its Role in the Intensification of Summer Rainfall Variability in the Southeastern United States. *Journal of Climate*, *24*(5), 1499–1506. https://doi.org/10.1175/2010JCLI3829.1

LIGA members, Anderson, P., Borisova, O., de Beaulieu, J.-L., de Vernal, A., Eiriksson, J., Funder, S., Gibbard, P., Hamilton, T., Harrison, S. P., Houmark-Nielsen, M., Huntley, B., Knudsen, K. L., Larsen, E., Maher, L. J., Matthews, J. V, Miller, G., Raukas, A., Reeh, N.,

… Ward, B. (1991). Report of 1st discussion group: The last interglacial in high latitudes of the Northern Hemisphere: Terrestrial and marine evidence. *Quaternary International*, *10–12*, 9–28. https://doi.org/https://doi.org/10.1016/1040-6182(91)90038-P

Limoges, A., de Vernal, A., & Van Nieuwenhove, N. (2014). Long-term hydrological changes in the northeastern Gulf of Mexico (ODP-625B) during the Holocene and late Pleistocene inferred from organic-walled dinoflagellate cysts. *Palaeogeography, Palaeoclimatology, Palaeoecology*, *414*, 178–191. https://doi.org/https://doi.org/10.1016/j.palaeo.2014.08.019

Lindstrom, S. (1990). Submerged Tree Stumps as Indicators of Mid-Holocene Aridity in the Lake Tahoe Region. *Journal of California and Great Basin Anthropology*, *12*(2), 146–157. http://www.jstor.org/stable/10.2307/27825419

Lora, J. M., & Ibarra, D. E. (2019). The North American hydrologic cycle through the last deglaciation. *Quaternary Science Reviews*, *226*, 105991. https://doi.org/https://doi.org/10.1016/j.quascirev.2019.105991

Lyle, M., Heusser, L., Ravelo, C., Andreasen, D., Olivarez Lyle, A., & Diffenbaugh, N. (2010). Pleistocene water cycle and eastern boundary current processes along the California continental margin. *Paleoceanography*, *25*(4). https://doi.org/https://doi.org/10.1029/2009PA001836

Mantua, N. J., & Hare, S. R. (2002). The Pacific Decadal Oscillation. In *Journal of Oceanography* (Vol. 58, Issue 1, pp. 35–44). https://doi.org/10.1023/A:1015820616384

Marcott, S. A., Shakun, J. D., Clark, P. U., & Mix, A. C. (2013). A Reconstruction of Regional and Global Temperature for the Past 11,300 Years. *Science*, *339*(6124), 1198–1201. https://doi.org/10.1126/science.1228026

Mauri, A., Davis, B. A. S., Collins, P. M., & Kaplan, J. O. (2014). The influence of atmospheric circulation on the mid-Holocene climate of Europe: a data–model comparison. *Climate of the Past*, *10*(5), 1925–1938. https://doi.org/10.5194/cp-10-1925-2014

Members, C. L. I. P. (2006). Last Interglacial Arctic warmth confirms polar amplification of climate change. *Quaternary Science Reviews*, *25*(13), 1383–1400. https://doi.org/https://doi.org/10.1016/j.quascirev.2006.01.033

Miller, G. H., Alley, R. B., Brigham-Grette, J., Fitzpatrick, J. J., Polyak, L., Serreze, M. C., & White, J. W. C. (2010). Arctic amplification: Can the past constrain the future? *Quaternary Science Reviews*, *29*(15–16), 1779–1790. https://doi.org/10.1016/j.quascirev.2010.02.008

Miller, I. M., Pigati, J. S., Scott Anderson, R., Johnson, K. R., Mahan, S. A., Ager, T. A., Baker, R. G., Blaauw, M., Bright, J., Brown, P. M., Bryant, B., Calamari, Z. T., Carrara, P. E., Cherney, M. D., Demboski, J. R., Elias, S. A., Fisher, D. C., Gray, H. J., Haskett, D. R., … Wilson, J. (2014). Summary of the Snowmastodon Project Special Volume: A high-elevation, multi-proxy biotic and environmental record of MIS 6–4 from the Ziegler Reservoir fossil site, Snowmass Village, Colorado, USA. *Quaternary Research*, *82*(3), 618–634. https://doi.org/https://doi.org/10.1016/j.yqres.2014.07.004

Montero-Serrano, J.-C., Bout-Roumazeilles, V., Carlson, A. E., Tribovillard, N., Bory, A., Meunier, G., Sionneau, T., Flower, B. P., Martinez, P., Billy, I., & Riboulleau, A. (2011). Contrasting rainfall patterns over North America during the Holocene and Last Interglacial as recorded by sediments of the northern Gulf of Mexico. *Geophysical Research Letters*, *38*(14). https://doi.org/https://doi.org/10.1029/2011GL048194

Morin, J., Block, P., Rajagopalan, B., & Clark, M. (2008). Identification of large scale climate patterns affecting snow variability in the eastern United States. *International Journal of Climatology*, *28*(3), 315–328. https://doi.org/https://doi.org/10.1002/joc.1534

Muhs, D. R., Ager, T. A., & Begét, J. E. (2001). Vegetation and paleoclimate of the last interglacial period, central Alaska. *Quaternary Science Reviews*, *20*(1), 41–61. https://doi.org/https://doi.org/10.1016/S0277-3791(00)00132-3

Ning, L., & Bradley, R. (2015). Winter Climate Extremes over the Northeastern United States and Southeastern Canada and Teleconnections with Large-Scale Modes of Climate Variability*. *Journal of Climate*, *28*, 2475–2493. https://doi.org/10.1175/JCLI-D-13-00750.1

Osman, M. B., Tierney, J. E., Zhu, J., Tardif, R., Hakim, G. J., King, J., & Poulsen, C. J. (2021). Globally resolved surface temperatures since the Last Glacial Maximum. *Nature*, *599*(7884), 239–244. https://doi.org/10.1038/s41586-021-03984-4

Oster, J.L., Ibarra, D.E., 2019, Glacial hydroclimate of western North America: Insights from proxy-model comparison and implications for Lake Bonneville. *Proceedings Volume: 2018 Lake Bonneville Geologic Conference and Short Course*, Lund, W.R., McKean, A.P., Bowman, S.D (eds) Utah Geological Survey Miscellaneous Publication 170.

Oster, J. L., Ibarra, D. E., Winnick, M. J., & Maher, K. (2015). Steering of westerly storms over western North America at the Last Glacial Maximum. *Nature Geoscience*, *8*(3), 201–205. https://doi.org/10.1038/ngeo2365

Otto-Bliesner, B. L., Brady, E. C., Zhao, A., Brierley, C. M., Axford, Y., Capron, E., Govin, A., Hoffman, J. S., Isaacs, E., Kageyama, M., Scussolini, P., Tzedakis, P. C., Williams, C. J. R., Wolff, E., Abe-Ouchi, A., Braconnot, P., Ramos Buarque, S., Cao, J., De Vernal, A., … Zheng, W. (2021). Large-scale features of Last Interglacial climate: Results from evaluating the lig127k simulations for the Coupled Model Intercomparison Project (CMIP6)-Paleoclimate Modeling Intercomparison Project (PMIP4). *Climate of the Past*, *17*(1), 63–94. https://doi.org/10.5194/cp-17-63-2021

Otto-Bliesner, B., Braconnot, P., Harrison, S., Lunt, D., Abe-Ouchi, A., Albani, S., Bartlein, P., Capron, E., Carlson, A., Dutton, A., Fischer, H., Goelzer, H., Govin, A., Haywood, A., Joos, F., LeGrande, A., Lipscomb, W., Lohmann, G., Mahowald, N., & Zhang, Q. (2017). The PMIP4 contribution to CMIP6 – Part 2: Two interglacials, scientific objective and experimental design for Holocene and Last Interglacial simulations. *Geosci. Model Dev.*, *10*, 3979–4003. https://doi.org/10.5194/gmd-10-3979-2017

Pewe, T. L., Berger, G. W., Westgate, J. A., Brown, P. M., & Leavitt, S. W. (1997). Eva interglaciation forest bed, unglaciated East-Central Alaska: Global warming 125,000 years ago. In T. L. Péwé, G. W. Berger, J. A. Westgate, P. M. Brown, & S. W. Leavitt (Eds.), *Eva interglaciation forest bed, unglaciated East-Central Alaska: global warming 125,000 years ago* (Vol. 319, p. 0). Geological Society of America. https://doi.org/10.1130/0-8137-2319-1.1

Pierce, K. L., Muhs, D. R., Fosberg, M. A., Mahan, S. A., Rosenbaum, J. G., Licciardi, J. M., & Pavich, M. J. (2011). A loess–paleosol record of climate and glacial history over the past two glacial–interglacial cycles (~150ka), southern Jackson Hole, Wyoming. *Quaternary Research*, *76*(1), 119–141. https://doi.org/https://doi.org/10.1016/j.yqres.2011.03.006

Pisias, N. G., Martinson, D. G., Moore, T. C., Shackleton, N. J., Prell, W., Hays, J., & Boden, G. (1984). High resolution stratigraphic correlation of benthic oxygen isotopic records spanning the last 300,000 years. *Marine Geology*, *56*(1), 119–136. https://doi.org/https://doi.org/10.1016/0025-3227(84)90009-4

Pisias, N. G., Mix, A. C., & Heusser, L. (2001). Millennial scale climate variability of the northeast Pacific Ocean and northwest North America based on radiolaria and pollen.

Quaternary Science Reviews, *20*(14), 1561–1576. https://doi.org/https://doi.org/10.1016/S0277-3791(01)00018-X

Reheis, M. C., Bright, J., Lund, S. P., Miller, D. M., Skipp, G., & Fleck, R. J. (2012). A half-million-year record of paleoclimate from the Lake Manix Core, Mojave Desert, California. *Palaeogeography, Palaeoclimatology, Palaeoecology*, *365–366*, 11–37. https://doi.org/https://doi.org/10.1016/j.palaeo.2012.09.002

Riboulleau, A., Bout-Roumazeilles, V., & Tribovillard, N. (2014). Controls on detrital sedimentation in the Cariaco Basin during the last climatic cycle: insight from clay minerals. *Quaternary Science Reviews*, *94*, 62–73. https://doi.org/https://doi.org/10.1016/j.quascirev.2014.04.023

Rodionov, S. N., Bond, N. A., & Overland, J. E. (2007). The Aleutian Low, storm tracks, and winter climate variability in the Bering Sea. *Deep Sea Research Part II: Topical Studies in Oceanography*, *54*(23), 2560–2577. https://doi.org/https://doi.org/10.1016/j.dsr2.2007.08.002

Rogers, J. (1990). Patterns of Low-Frequency Monthly Sea Level Pressure Variability (1899–1986) and Associated Wave Cyclone Frequencies. *Journal of Climate*, *3*, 1364–1379. https://doi.org/10.1175/1520-0442(1990)003<1364:POLFMS>2.0.CO;2

Scheff, J. (2018). Drought Indices, Drought Impacts, CO2, and Warming: a Historical and Geologic Perspective. *Current Climate Change Reports*, *4*(2), 202–209. https://doi.org/10.1007/s40641-018-0094-1

Schmidt, G. A., Annan, J. D., Bartlein, P. J., Cook, B. I., Guilyardi, E., Hargreaves, J. C., Harrison, S. P., Kageyama, M., Legrande, A. N., Konecky, B., Lovejoy, S., Mann, M. E., Masson-Delmotte, V., Risi, C., Thompson, D., Timmermann, A., & Yiou, P. (2014). Using palaeo-climate comparisons to constrain future projections in CMIP5. *Climate of the Past*, *10*(1), 221–250. https://doi.org/10.5194/cp-10-221-2014

Schmidt, M. W., & Spero, H. J. (2011). Meridional shifts in the marine ITCZ and the tropical hydrologic cycle over the last three glacial cycles. *Paleoceanography*, *26*(1). https://doi.org/https://doi.org/10.1029/2010PA001976

Schneider, U., Becker, A., Finger, P., Meyer-Christoffer, A., Rudolf, B., Ziese, M., 2011. GPCC full data reanalysis version 6.0 at 0.5◦: Monthly landsurface precipitation from rain-gauges built on gts-based and historic data.

Schweger, C. E., & Matthews, J. V. (1991). The last (Koy-Yukon) interglaciation in the Yukon: Comparisons with holocene and interstadial pollen records. *Quaternary International*, *10–12*, 85–94. https://doi.org/https://doi.org/10.1016/1040-6182(91)90042-M

Sharpe, S. E., & Bright, J. (2014). A high-elevation MIS 5 hydrologic record using mollusks and ostracodes from Snowmass Village, Colorado, USA. *Quaternary Research*, *82*(3), 604–617. https://doi.org/https://doi.org/10.1016/j.yqres.2014.01.014

Springer, G. S., Rowe, H. D., Hardt, B., Cheng, H., & Edwards, R. L. (2014). East central North America climates during marine isotope stages 3–5. *Geophysical Research Letters*, *41*(9), 3233–3237. https://doi.org/https://doi.org/10.1002/2014GL059884

Suh, Y. J., Diefendorf, A. F., Freimuth, E. J., & Hyun, S. (2020). Last interglacial (MIS 5e) and Holocene paleohydrology and paleovegetation of midcontinental North America from Gulf of Mexico sediments. *Quaternary Science Reviews*, *227*, 106066. https://doi.org/https://doi.org/10.1016/j.quascirev.2019.106066

Sundqvist, H. S., Kaufman, D. S., McKay, N. P., Balascio, N. L., Briner, J. P., Cwynar, L. C., Sejrup, H. P., Seppä, H., Subetto, D. A., Andrews, J. T., Axford, Y., Bakke, J., Birks, H. J.

B., Brooks, S. J., de Vernal, A., Jennings, A. E., Ljungqvist, F. C., Rühland, K. M., Saenger, C., … Viau, A. E. (2014). Arctic Holocene proxy climate database – new approaches to assessing geochronological accuracy and encoding climate variables. *Climate of the Past*, *10*(4), 1605–1631. https://doi.org/10.5194/cp-10-1605-2014

Swain, D. L., Tsiang, M., Haugen, M., Singh, D., Charland, A., Rajaratnam, B., & Diffenbaugh, N. S. (2014). THE EXTRAORDINARY CALIFORNIA DROUGHT OF 2013/2014: CHARACTER, CONTEXT, AND THE ROLE OF CLIMATE CHANGE. *Bulletin of the American Meteorological Society*, *95*(9), S3–S7. http://proxy.library.vanderbilt.edu/login?url=https://www.proquest.com/scholarly-journals/extraordinary-california-drought-2013-2014/docview/1623231385/se-2?accountid=14816

Swann, A. L. S., Fung, I. Y., Liu, Y., & Chiang, J. C. H. (2014). Remote Vegetation Feedbacks and the Mid-Holocene Green Sahara. *Journal of Climate*, *27*(13), 4857–4870. https://doi.org/10.1175/JCLI-D-13-00690.1

Tabor, C., Otto-Bliesner, B., & Liu, Z. (2020). Speleothems of South American and Asian Monsoons Influenced by a Green Sahara. *Geophysical Research Letters*, *47*(22), e2020GL089695. https://doi.org/https://doi.org/10.1029/2020GL089695

Tarnocai, C. (1990). Paleosols of the Interglacial Climates in Canada. *Géographie Physique et Quaternaire*, *44*(3), 363–374. https://doi.org/https://doi.org/10.7202/032836ar

Teed, R. (2000). A >130,000-Year-Long Pollen Record from Pittsburg Basin, Illinois. *Quaternary Research*, *54*(2), 264–274. https://doi.org/https://doi.org/10.1006/qres.2000.2161

Thompson, A. J., Zhu, J., Poulsen, C. J., Tierney, J. E., & Skinner, C. B. (2022). Northern Hemisphere vegetation change drives a Holocene thermal maximum. *Science Advances*, *8*(15), eabj6535. https://doi.org/10.1126/sciadv.abj6535

Thompson, R., Whitlock, C., Bartlein, P., & Al., E. (1993). Climatic Changes in the Western United States since 18,000 yr B.P. In H. Wright, J. Kutzbackm, I. Webb, T, W. Ruddiman, S.-P. FA, & P. Bartlein (Eds.), *Global Climates Since the Last Glacial Maximum* (pp. 468–513). University of Minnesota Press.

Tierney, J. E., Poulsen, C. J., Montañez, I. P., Bhattacharya, T., Feng, R., Ford, H. L., Hönisch, B., Inglis, G. N., Petersen, S. V, Sagoo, N., Tabor, C. R., Thirumalai, K., Zhu, J., Burls, N. J., Foster, G. L., Goddéris, Y., Huber, B. T., Ivany, L. C., Turner, S. K., … Zhang, Y. G. (2020). Past climates inform our future. *Science*, *370*(6517), eaay3701. https://doi.org/10.1126/science.aay3701

Tingstad, A., Groves, D., & Lempert, R. (2014). Paleoclimate Scenarios to Inform Decision Making in Water Resource Management: Example from Southern California's Inland Empire. *Journal of Water Resources Planning and Management*, *140*, 4014025. https://doi.org/10.1061/(ASCE)WR.1943-5452.0000403

Trenberth, K. E. (2011). Changes in precipitation with climate change. *Climate Research*, *47*(1–2), 123–138. https://doi.org/10.3354/cr00953

Whitlock, C., & Bartlein, P. J. (1997). Vegetation and climate change in northwest America during the past 125 kyr. *Nature*, *388*(6637), 57–61. https://doi.org/10.1038/40380

Wise, E. K. (2016). Five centuries of U.S. West Coast drought: Occurrence, spatial distribution, and associated atmospheric circulation patterns. *Geophysical Research Letters*, *43*(9), 4539–4546. https://doi.org/10.1002/2016GL068487

Wong, C. I., Potter, G. L., Montañez, I. P., Otto-Bliesner, B. L., Behling, P., & Oster, J. L. (2016). Evolution of moisture transport to the western U.S. during the last deglaciation. *Geophysical Research Letters*, *43*(7), 3468–3477. https://doi.org/https://doi.org/10.1002/2016GL068389

Woodhouse, C., Lukas, J., Morino, K., Meko, D., & Hirschboeck, K. (2016). *Using the Past to Plan for the Future—The Value of Paleoclimate Reconstructions for Water Resource Planning* (pp. 161–182). https://doi.org/10.1201/b19534-12

Woolfenden, W. B. (2003). A 180,000-year pollen record from Owens Lake, CA: terrestrial vegetation change on orbital scales. *Quaternary Research*, *59*(3), 430–444. https://doi.org/https://doi.org/10.1016/S0033-5894(03)00033-4

Wyatt, P. (1990). Amino Acid Evidence Indicating Two or More Ages of Pre-Holocene Nonglacial Deposits In Hudson Bay Lowland, Northern Ontario. *Géographie Physique et Quaternaire*, *44*(3), 389–393. https://doi.org/https://doi.org/10.7202/032838ar

Paleoceanography and Paleoclimatology

Supporting Information for

North American hydroclimate during past warm states: A proxy network-model comparison for the Last Interglacial and the mid-Holocene

C. B. de Wet[1], D. E. Ibarra[2], B. K. Belanger[1], J. L. Oster[1]

[1]Department of Earth and Environmental Sciences, Vanderbilt University, Nashville, TN, USA.

[2]Earth, Environmental, and Planetary Sciences, Brown University, Providence, RI, USA.

Contents of this file

Additional Supporting Information (Files uploaded separately)

Tables S1 and S2

Introduction

This file includes maps of annual average precipitation (%ΔP) and runoff anomalies (%ΔP-ET) from PIMP4 model simulations and moisture sensitive proxy networks for the mid-Holocene (MH) (Figure S1 and S3) and Last Interglacial (LIG) (Figure S2 and S4). It also includes information about the proxy records included in our MH (Table S1) and LIG (Table S2) networks and about the PMIP4 models used in our analyses (Table S3). Finally, it includes the calculated agreement coefficients (Gwet's AC2, Cohen's kappa, and Gwet's AC1) for categorical comparison between the PMIP4 models and the MH (Table S4) and LIG (Table S5) proxy networks, as well as for the western US proxy network from Hermann et al. (2018).

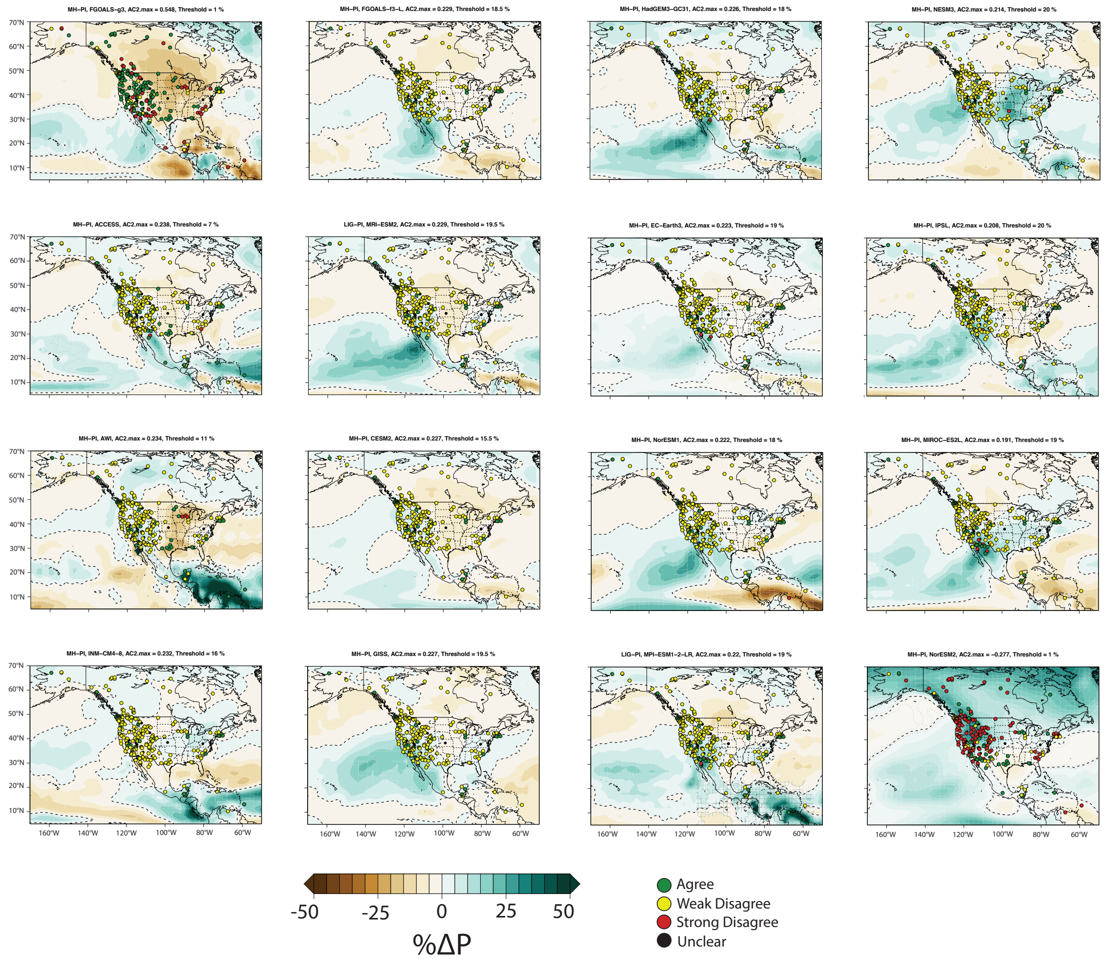

Figure S1. Annual MH-PI precipitation anomaly (%ΔP) for PMIP4 models with MH proxy network plotted based on agreement with ensemble climatology. Dark gray dashed lines denote the boundary between positive and negative precipitation anomalies. Light gray dotted lines denote the threshold for the change in precipitation to be considered wetter, drier, or unchanged based on optimized agreement with the proxy network. The precipitation anomaly for NorESM2 is -100 to 100%.

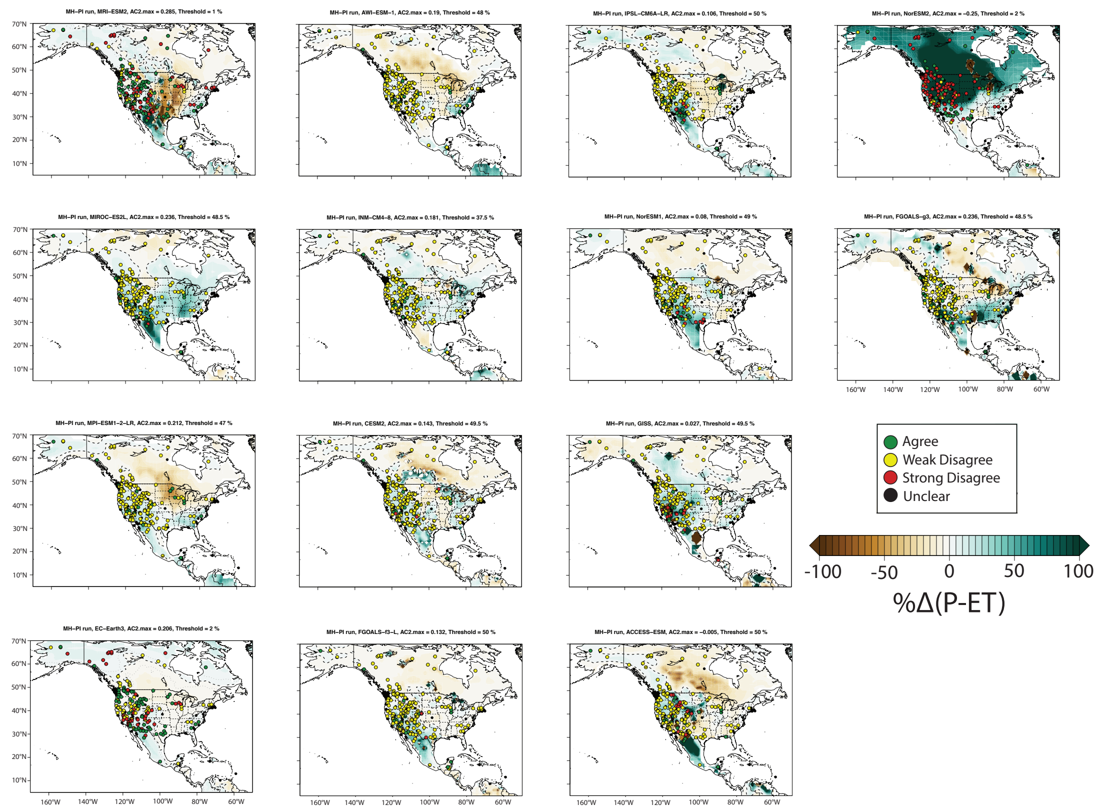

Figure S2. Annual MH-PI runoff anomaly (%ΔP-ET) for PMIP4 models with MH proxy network plotted based on agreement with ensemble climatology. Dark gray dashed lines and light gray dotted lines same as in Figure S1.

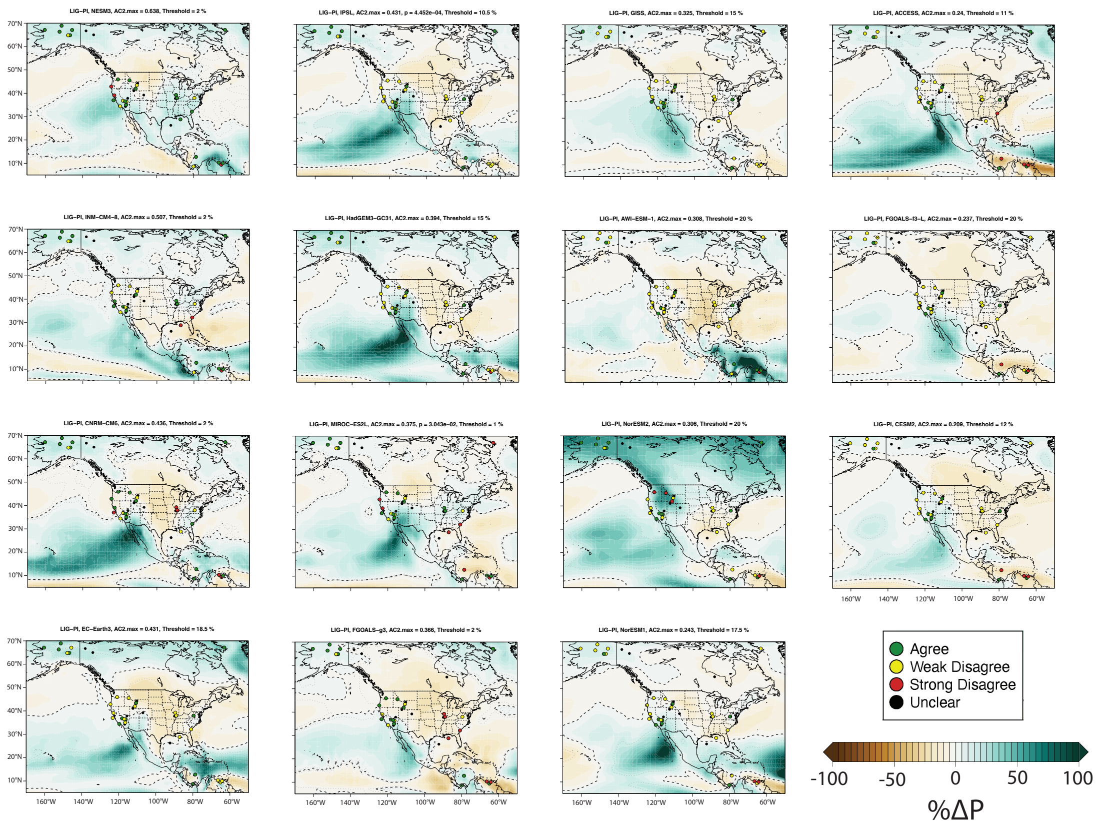

Figure S3. Annual LIG-PI precipitation anomaly (%ΔP) for PMIP4 models with LIG proxy network plotted based on agreement with ensemble climatology. Dark gray dashed lines and light gray dotted lines same as in Figure S1.

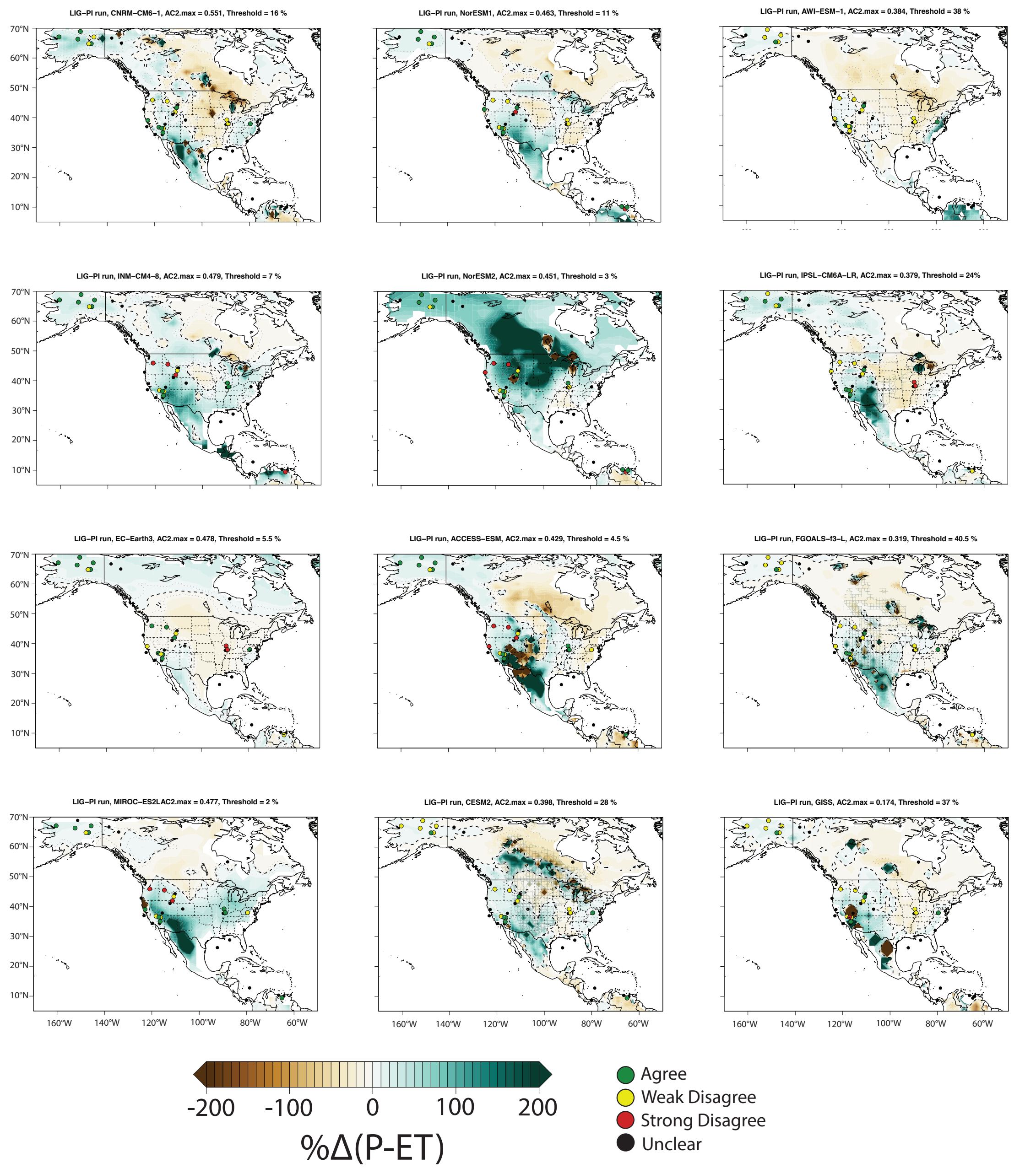

Figure S4. Annual LIG-PI runoff anomaly (%ΔP-ET) for PMIP4 models with LIG proxy network plotted based on agreement with ensemble climatology. Dark gray dashed lines and light gray dotted lines same as in Figure S1.

Table S1. The mid-Holocene proxy network.

(Uploaded separately.)

Table S2. The Last Interglacial proxy network.

(Uploaded separately.)

Table S3. Description of PMIP4 models used in this study.

Model	Experiments and outputs	Number of grid cells (lat.)	Number of grid cells (lon.)	Citation for model description	Notes
ACCESS-ESM1-5	*piControl - pr, evspsbl; midHolocene - pr, evspsbl; lig127k - pr, evspsbl*	145	192	Ziehn et al. (2017, 2020)	Fixed vegetation with interactive leaf area index, prescribed aerosols
AWI-ESM-1-1-LR	*piControl - pr, evspsbl; midHolocene - pr, evspsbl; lig127k - pr, evspsbl*	96	192	Sidorenko et al. (2015)	Interactive vegetation
CESM2	*piControl - pr, evspsbl; midHolocene - pr, evspsbl; lig127k - pr, evspsbl*	192	288	Danabasoglu et al. (2020)	Prescribed potential vegetation (crops and urban areas removed), interactive phenology, simulated dust
CNRM-CM6-1	*piControl - pr, evspsbl; lig127k - pr, evspsbl*	128	256	Voldoire et al. (2019), Decharme et al. (2019)	PI atm. GHGs, prescribed vegetation and aerosols
EC-Earth3-LR	*piControl - pr, evspsbl; midHolocene - pr, evspsbl; lig127k - pr, evspsbl*	160	320	Zhang et al. (2020) (for lig127K)	Prescribed vegetation and aerosols
FGOALS-f3-L	*piControl - pr, evspsbl; midHolocene - pr, evspsbl; lig127k - pr, evspsbl*	180	288	Zheng et al. (2020) (for lig127K)	Prescribed vegetation and aerosols
FGOALS g3	*piControl - pr, evspsbl; midHolocene - pr, evspsbl; lig127k - pr, evspsbl*	80	180	Zheng et al. (2020) (for lig127K)	Prescribed vegetation and aerosols
GISS-E2-1-G	*piControl - pr, evspsbl; midHolocene - pr, evspsbl; lig127k - pr, evspsbl*	90	144	Kelley et al. (2020)	Prescribed vegetation
HadGEM3-GC31-LL	*piControl - pr; midHolocene - pr; lig127k - pr*	144	192	Kuhlbrodt et al. (2018), Williams et al. (2017)	Prescribed vegetation and aerosols
INM-CM4-8	*piControl - pr, evspsbl; midHolocene - pr, evspsbl; lig127k - pr, evspsbl*	120	180	Volodin et al. (2018)	Prescribed vegetation, simulated dust and sea salt
IPSL-CM6A-LR	*piControl - pr, evspsbl; midHolocene - pr, evspsbl; lig127k - pr, evspsbl*	143	144	Boucher et al. (2020)	Prescribed vegetation, interactive phenology, prescribed aerosols
MIROC-ES2L	*piControl - pr, evspsbl; midHolocene - pr, evspsbl; lig127k - pr, evspsbl*	64	128	Hajima et al. (2020)	Prescribed vegetation and aerosols
MPI-ESM1-2-LR	*piControl - pr, evspsbl; midHolocene - pr, evspsbl*	96	192	Giogetta et al. (2013)	Interactive vegetation, prescribed aerosols
MRI-ESM2	*piControl - pr, evspsbl; midHolocene - pr, evspsbl*	160	320	Yukimoto et al. (2019)	
NESM3	*piControl - pr; midHolocene - pr; lig127k - pr*	96	192	Cao et al. (2018)	Interactive vegetation, prescribed aerosols
NorESM1-F	*piControl - pr, evspsbl; midHolocene - pr, evspsbl; lig127k - pr, evspsbl*	96	144	Guo et al. (2019)	Prescribed vegetation and aerosols
NorESM2-LM	*piControl - pr, evspsbl; midHolocene - pr, evspsbl; lig127k - pr, evspsbl*	96	144	Seland et al. (2020)	Prescribed vegetation and aerosols

Table S4. Gwet's AC2, Cohen's kappa (K_w), and Gwet's AC1 values with associated statistical significance and optimized precipitation threshold for comparisons between the mid-Holocene proxy network and annual precipitation from PMIP4 mid-Holocene simulations.

	AC2	p value	Precip. threshold (%)		Kw	Significance	Precipitation threshold (%)		AC1	p value	Precip. threshold (%)
FGOALS-g3	0.55	0	1		0.13	Not Sig	5		0.51	0.00E+00	1
ACCESS-ESM	0.24	8.47E-11	7		0.08	Sig	6		0.00	1.04E+00	1
AWI-ESM-1	0.23	6.42E-11	11		0.07	Not Sig	7		0.06	2.40E-01	1
INM-CM4-8	0.23	2.95E-11	16		0.03	Not Sig	10		0.17	1.32E-03	1
FGOALS-f3-L	0.23	6.01E-11	18.5		0.08	Not Sig	2		0.20	1.10E-04	1
MRI-ESM2	0.23	6.01E-11	19.5		0.19	Sig	1		0.15	2.29E-03	1
CESM2	0.23	8.45E-11	15.5		0.02	Not Sig	6		-0.01	1.18E+00	1
GISS-E2-1-G	0.23	8.45E-11	19.5		0.04	Not Sig	2		-0.06	1.84E+00	1
HadGEM3-GC31-LL	0.23	2.44E-10	18		0.11	Sig	5		0.01	8.40E-01	1
EC-Earth3-LR	0.22	8.62E-10	19		0.16	Sig	2		0.20	1.18E-04	1
NorESM1-F	0.22	5.04E-10	18		0.08	Sig	7		-0.03	1.54E+00	1
MPI-ESM1-2-LR	0.22	9.81E-10	19		0.15	Sig	6		0.04	4.40E-01	1
NESM3	0.21	4.20E-09	20		0.09	Sig	4		0.05	2.70E-01	1
IPSL-CM6A-LR	0.21	3.48E-09	20		0.11	Sig	3		0.04	3.50E-01	1
MIROC-ES2L	0.19	3.18E-07	19		0.07	Not Sig	4		0.01	8.00E-01	1
NorESM2-LM	-0.28	2.00E+00	1		-0.04	Not Sig	1		-0.09	1.96E+00	1

Table S5. Gwet's AC2, Cohen's kappa (K_w), and Gwet's AC1 values with associated statistical significance and optimized precipitation threshold for comparisons between the Last Interglacial proxy network and annual precipitation from PMIP4 Last Interglacial simulations.

	AC2	p value	Precip. threshold (%)		Kw	Significance	Precipitation threshold (%)		AC1	p value	Precip. threshold (%)
NESM3	0.64	1.42E-05	2		0.4	Sig	2		0.55	2.00E-04	2
INM-CM4-8	0.51	1.50E-03	2		0.35	Sig	2		0.42	5.90E-03	2
CNRM-CM6	0.44	7.70E-03	2		0.35	Sig	2		0.42	4.60E-03	2
EC-Earth3-LR	0.43	2.00E-04	18.5		0.31	Sig	8		0.34	2.25E-02	4
IPSL-CM6A-LR	0.43	4.00E-04	10.5		0.19	Not Sig	4		0.32	2.64E-02	1
HadGEM3-GC31-LL	0.39	2.30E-03	15		0.14	Not Sig	19		0.21	1.45E-01	11
MIROC-ES2L	0.38	3.04E-02	1		0.19	Not Sig	1		0.39	9.00E-03	1
FGOALS-g3	0.37	3.24E-02	2		0.36	Sig	2		0.4	6.60E-03	2
GISS-E2-1-G	0.32	2.50E-03	15		0.17	Not Sig	4		0.21	1.64E-01	2
AWI-ESM-1	0.31	1.10E-02	20		0.15	Not Sig	3		0.2	1.69E-01	2
NorESM2-LM	0.31	4.78E-02	20		0.09	Not Sig	20		0.21	1.38E-01	20
NorESM1-F	0.24	8.38E-02	17.5		0.11	Not Sig	12.5		0.17	2.39E-01	1
ACCESS-ESM1-5	0.24	1.38E-01	11		0.14	Not Sig	11		0.15	2.99E-01	3
FGOALS-f3-L	0.24	9.16E-02	20		0.13	Not Sig	1		0.16	2.76E-01	1
CESM2	0.21	1.70E-01	12		0.05	Not Sig	12		0.13	3.77E-01	1

Table S6. Gwet's AC2, Cohen's kappa (K_w), and Gwet's AC1 values with associated statistical significance and optimized precipitation threshold for comparisons between the mid-Holocene proxy network from Hermann et al. (2018) and annual precipitation from PMIP4 mid-Holocene simulations.

	AC2	p value	Precip. threshold (%)		Kw	Significance	Precip. threshold (%)		AC1	p value	Precip. threshold (%)
FGOALS-g3	0.62	0.00E+00	1		0.21	Sig	2		0.55	0.00E+00	1
INM-CM4-8	0.28	8.40E-10	15		0	Not Sig	15		0.19	3.87E-03	1
AWI-ESM-1	0.28	8.40E-10	16.5		0.04	Not Sig	7		-0.09	1.90E+00	7
CESM2	0.28	8.40E-10	14.5		0.05	Not Sig	5		-0.1	1.93E+00	14.5
EC-Earth3-LR	0.28	1.55E-09	19		0.24	Sig	2		0.23	3.00E-04	1
GISS-E2-1-G	0.28	8.40E-10	19.5		0.12	Sig	2		-0.08	1.84E+00	2
NorESM1-F	0.28	8.40E-10	18		0.16	Sig	7		-0.06	1.75E+00	7
FGOALS-f3-L	0.28	5.81E-10	18.5		0.21	Sig	2		0.17	9.46E-03	1
ACCESS-ESM1-5	0.28	8.40E-10	18.5		0.05	Not Sig	6		-0.08	1.86E+00	7
MRI-ESM2	0.28	5.81E-10	19.5		0.23	Sig	1		0.13	4.41E-02	1
NESM3	0.27	9.69E-09	19		0.15	Sig	1		0.1	9.45E-02	1
MPI-ESM1-2-LR	0.27	2.77E-09	19		0.17	Sig	6		-0.05	1.66E+00	1
HadGEM3-GC31-LL	0.27	3.38E-09	17		0.16	Sig	6		-0.05	1.62E+00	9
IPSL-CM6A-LR	0.25	6.63E-08	20		0.16	Sig	7		-0.03	1.43E+00	1
MIROC-ES2L	0.23	2.12E-06	19		0.2	Sig	3		0	1.04E+00	1
NorESM2-LM	-0.39	2.00E+00	1		-0.02	Not Sig	1		-0.18	2.00E+00	1